Structural Biology and Molecular Biophysics

A parametrized two-domain thermodynamic model explains diverse mutational effects on protein allostery

Zhuang Liu, Thomas Gillis, Srivatsan Raman, Qiang Cui

Department of Physics, Boston University, Boston, United States • Department of Biochemistry, University of Wisconsin, Madison, United States • Department of Chemistry, University of Wisconsin, Madison, United States • Department of Bacteriology, University of Wisconsin, Madison, United States • Department of Chemistry, Boston University, Boston, United States

Reviewed Preprint

Revised by authors after peer review.

About eLife's process

Reviewed preprint version 2
April 16, 2024 (this version)

Reviewed preprint version 1
December 19, 2023

Sent for peer review
September 18, 2023

Posted to preprint server
August 26, 2023

Abstract

New experimental findings continue to challenge our understanding of protein allostery. Recent deep mutational scanning study showed that allosteric hotspots in the tetracycline repressor (TetR) and its homologous transcriptional factors are broadly distributed rather than spanning well-defined structural pathways as often assumed. Moreover, hotspot mutation-induced allostery loss was rescued by distributed additional mutations in a degenerate fashion. Here, we develop a two-domain thermodynamic model for TetR, which readily rationalizes these intriguing observations. The model accurately captures the in vivo activities of various mutants with changes in physically transparent parameters, allowing the data-based quantification of mutational effects using statistical inference. Our analysis reveals the intrinsic connection of intra- and inter-domain properties for allosteric regulation and illustrate epistatic interactions that are consistent with structural features of the protein. The insights gained from this study into the nature of two-domain allostery are expected to have broader implications for other multidomain allosteric proteins.

eLife assessment

The study presents **valuable** findings where two-domain thermodynamic model for TetR accurately predicts in vivo phenotype changes brought about as a result of various mutations. The evidence provided is **compelling** and features the first innovative observations with a computational model that captures the structural behavior, much more than the current single-domain models.

Introduction

Allostery, a fundamental regulatory mechanism of biomolecular functions, is prevalent in life processes Bacon (1965); Koshland Jr et al. (1966); Changeux and Edelstein (2005); Cui and Karplus (2008); Motlagh et al. (2014); Yu and Koshland Jr (2001); Süel et al. (2003); Dokholyan (2016). The long-range signaling of allostery makes it a fascinating phenomenon, in which binding of an effector molecule (ligand) at the allosteric site alters the function of a distal active site Dokholyan (2016); Leander et al. (2020); Peracchi and Mozzarelli (2011); Wodak et al. (2019). Current descriptions of allostery can be largely cast into two categories: one adopts a mechanical view, focusing on the propagation of conformational distortions from the allosteric site to the active site Wang et al. (2020); Lockless and Ranganathan (1999); Daily and Gray (2009); Rodriguez et al. (2010); Lee et al. (2008); Walker et al. (2020); the other emphasizes the thermodynamic aspect of the problem, high-lighting the effect of ligand binding on shifting the protein population among pre-existing conformational states characterized by different ligand binding affinities and active site properties (e.g., the classic MWC model) Bacon (1965); Koshland Jr et al. (1966); Changeux and Edelstein (2005); Cui and Karplus (2008); Sevvana et al. (2012); Takeuchi et al. (2019); Marzen et al. (2013). Models based on both perspectives have provided insights into the function of prototypical allosteric systems thanks to decades of combined efforts of experiment, computation and theory Cui and Karplus (2008); Motlagh et al. (2014); Dokholyan (2016); Marzen et al. (2013); Changeux (2012); Guo and Zhou (2016); Schueler-Furman and Wodak (2016); Reichheld et al. (2009); Xu et al. (2003); Nierzwicki et al. (2021); East et al. (2019). Of note, these two perspectives of allostery are complementary rather than contradictory to each other Liu and Nussinov (2016). The conformational coupling between spatially distant functional sites (allosteric site and active site) plays a vital role in regulating allosteric function, allowing for the transmission of signals from one site to the other Zhang et al. (2020). While the mechanical view primarily seeks to identify the structural basis for signal transduction, it is implicitly assumed within the population shift perspective, which offers a comprehensive and quantitative description of allostery Szabo and Karplus (1972); Viappiani et al. (2014); Henry et al. (2020); Eaton (2022).

In recent years, a thermodynamic model referred to as the ensemble allosteric model (EAM) has been applied to conceptualize protein allostery in terms of intra- and inter-domain properties, with the latter explicitly quantifying the energetic coupling between distant functional sites Motlagh et al. (2014); Wodak et al. (2019); Hilser et al. (2012). This framework is consistent with the observation that allosteric proteins often partition different activities into distinct domains, such as the ligand- and DNA-binding domains in transcription factors and the effector-binding and catalytic domains in enzymes Ramos et al. (2005); Tzeng and Kalodimos (2012); Velyvis et al. (2007); Lipscomb and Kantrowitz (2012). Such thermodynamic approach finds broad applicability across proteins in general, as it has been proposed that all proteins are potentially allosteric Zhang et al. (2020); Gunasekaran et al. (2004). Consequently, this raises intriguing questions about the nature of allostery. For instance, do intrinsic connections exist between the intra- and inter-domain properties of a protein, given the highly cooperative nature of allosteric networks? What roles do sequence and structure play in synergistically determining these properties? Furthermore, what are the parameters within the model that are most essential to the accurate description of realistic allosteric systems, especially prediction of activity upon multiple mutations? To answer these questions and deepen our understanding of allosteric regulation, it is essential to parameterize and test the thermodynamic model using comprehensive mutational data, a topic that still requires further exploration Leander et al. (2020, 2022).

A critical test of any thermodynamic model is whether it can explain the effect of mutations on allosteric signaling. Deep mutational scanning (DMS) analysis has emerged as a powerful function-centric approach over the past decade, which measures the impact of all possible single mutations

Fowler et al. (2010); Fowler and Fields (2014); Sarkisyan et al. (2016); Flynn et al. (2019); Starr et al. (2020); Huss et al. (2021). The methodology provides an unbiased way of identifying critical residues for protein allostery and generates extensive data for validating existing computational and theoretical models. Along this line, recent DMS study of four homologous bacterial transcription factors (TFs) in the TetR family (TetR, TtgR, MphR and RolR) revealed that the residues critical for allosteric signaling (hotspots) in these TFs are broadly distributed with no apparent structural link to either the allosteric or the active site Leander et al. (2022); Tack et al. (2021); Faure et al. (2022); Jones et al. (2020); McCormick et al. (2021). This contrasts the commonly held view that hotspot residues tend to form well-defined pathways linking the two sites Süel et al. (2003); Ota and Agard (2005); Strickland et al. (2008); Reynolds et al. (2011); Amor et al. (2016); the observations also hinted at common molecular rules of allostery in the TetR family of TFs Cuthbertson and Nodwell (2013); Fukami-Kobayashi et al. (2003). Moreover, systematic analysis of higher order TetR mutants in the background of five noninducible ("dead") mutants revealed remarkable functional plasticity in allosteric regulation Leander et al. (2020). Specifically, the loss of inducibility due to the mutations of allostery hotspots could be rescued (restored wildtype-like inducibility) by additional mutations, and different dead mutations exhibit varying numbers of rescuing mutations, which are usually distal and lacking any obvious structural rationale.

While the identification of broadly distributed dead and rescuing mutations in these studies is exciting, such qualitative activity characterization of mutants (inducible and noninducible at a given ligand concentration) prevents a deeper mechanistic understanding of the observation. In fact, mutations exert a graded impact on the allosteric signaling of the TFs; i.e., the expression level of the regulated gene varies among both inducible and noninducible mutants in a continuous, ligand-concentration dependent manner. The nuanced mutational effect on allosteric regulation is linked apparently to the equilibria among different conformational and binding states of the mutant TF, which are determined by the allosteric parameters (intra- and inter-domain properties). Therefore, mapping the mutants onto the parameter space of a biophysical model by exploiting additional experimental data (see below) is crucial for elucidating the observed allosteric phenomena in a comprehensive and physically transparent manner.

In this study, we develop a two-domain statistical thermodynamic model for TetR, in which the protein is generically divided into ligand- and DNA-binding domains (LBD and DBD). Our model incorporates three essential biophysical parameters that capture the intra- and inter-domain properties of the protein, as elaborated in the subsequent section. The model readily rationalizes the myriad ways that mutations can perturb allostery as observed in the aforementioned DMS measurements, by revealing that mutations perturbing intra- and inter-domain properties can lead to similar TF inducibilities at a single ligand concentration. Moreover, the model elucidates the distinct influences of these parameters on the complete induction curve, serving as a diagnostic tool for dissecting the intricate allosteric effects of mutations. We validate the model by accurately describing the induction curves of a comprehensive set of TetR mutants, thereby enabling the quantification of mutational effects and epistatic interactions Daber et al. (2011); Chure et al. (2019). The insights from this combined theoretical and experimental investigation of TetR allostery are expected to generally apply to other two-domain allosteric systems, such as transcription factors like catabolite activator protein (CAP) Tzeng and Kalodimos (2012), receptors like pentameric ligand-gated ion channels (pLGICs) Sauguet et al. (2015); Hu et al. (2020), and allosteric enzymes like aspartate transcarbamoylase (ATCase) Lipscomb and Kantrowitz (2012); Velyvis et al. (2007).

Results

Overview of the two-domain thermodynamic model of allostery

As shown in ***Figure 1A and B***, TetR can be generically divided into a LBD and a DBD, disregarding its homodimeric nature Leander et al. (2020); Takeuchi et al. (2019); Reichheld et al. (2009); Leander et al. (2022); Yuan et al. (2022); Scholz et al. (2004). In the same vein of the classic allostery models Bacon (1965); Koshland Jr et al. (1966), each domain features two (the relaxed/inactive and tense/active) conformations that differ in free energies and binding affinities. For the simplicity and mechanistic clarity of the model, we assume negligible binding affinity of the LBD to the lig- and and the DBD to DNA in their inactive conformations and consider competent binding only for the active ones. Each domain must overcome a free energy increase to transition from the inactive to the active conformation (ε_L for LBD and ε_D for DBD). Importantly, the two domains are allosterically coupled, in that there is a free energy penalty γ when both domains adopt the active conformations simultaneously. For example, when the ligand binds to the LBD, selecting its active conformation, it discourages the active conformation of the DBD and therefore DNA binding. This anti-cooperativity establishes the foundation for allosteric regulation in TetR.

Accordingly, there are four possible conformational states of TetR, namely $L_I\ D_I$, $L_A\ D_I$, $L_I\ D_A$ and $L_A\ D_A$, with L/D and I/A denoting LBD/DBD and inactive/active conformation, respectively (see ***Figure 1B*** and the upper four states of ***Figure 1D***). Binding of ligand/operator to the active LBD/DBD further lowers the free energy of the corresponding state in a concentration dependent manner following the standard formulation of binding equilibrium (see the lower three states of ***Figure 1D***). The regulatory mechanism of TetR allostery can then be qualitatively explained by the schematics in ***Figure 1C and D***. Without the ligand, wildtype (WT) repressor predominantly binds to the operator sequence, which obstructs the binding of RNA polymerase (RNAP) to the adjacent promoter of the regulated gene (***Figure 2—figure Supplement 1A***). In the presence of ligand (inducer) at a sufficiently high concentration, the ligand-bound $L_A\ D_I$ state (L-$L_A\ D_I$) has the lowest free energy compared with other possible (DNA-bound) states, thus the repressor predominantly releases the operator upon ligand binding, enabling the expression of downstream genes (***Figure 1C*** and ***Figure 2—figure Supplement 1A***).

Mutations perturb the three biophysical parameters (ε_D, ε_L and γ) and hence the free energy landscape (***Figure 1***D), leading to changes in TetR function. The three limiting scenarios are depicted in ***Figure 1***D: 1. when a mutation significantly increases ε_L, it raises the free energy of the L-$L_A\ D_I$ state relative to the DNA-bound state $L_I\ D_A$ -D, which results in a dead (noninducible) phenotype; 2. when a mutation substantially decreases ε_D, it raises the free energy of the L-$L_A\ D_I$ state relative to both DNA-bound states ($L_I\ D_A$ -D and L-$L_A\ D_A$ -D), also leading to a dead mutant; 3. mutations that decrease γ greatly lower the free energy of the double-bound state (L-$L_A\ D_A$ -D) relative to L-$L_A\ D_I$, again leading to the suppression of induction. Therefore, these schemes highlight that hotspot mutations can disrupt allostery by perturbing either intra- (ε_D, ε_L) or inter-domain (γ) properties. Functional readouts like DMS can help distinguish these mechanistic differences at the biophysical level. Notably, mutations mainly perturbing ε_D or ε_L do not have to lie on the structural pathways linking the allosteric and active sites, which explains the broad hotspot distributions observed in the DMS measurement Leander et al. (2020); Reichheld et al. (2009); Leander et al. (2022); Scholz et al. (2004). In general, a dead mutation is likely of mixed nature, as long as its effect on the free energy landscape promotes the dominance of the DNA-bound states. Likewise, rescuing mutations may restore WT-like inducibility by modifying intra- and inter-domain energetics in various ways, as far as the dominance of the L-$L_A\ D_I$ state is re-established, rationalizing the broad rescuing mutation distributions. Naturally, the rescuability

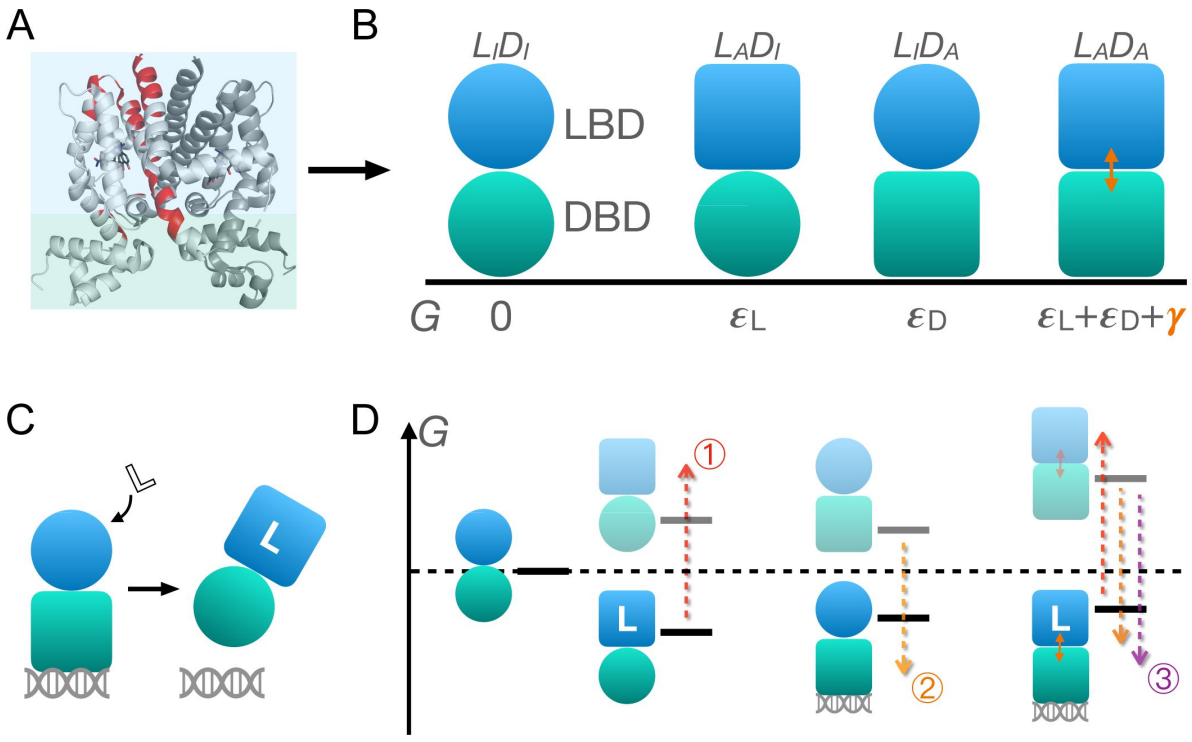

Figure 1.

Schematic illustration of the two-domain statistical thermodynamic model of TetR allostery. (A) The crystal structure of TetR(B) in complex with minocycline and magnesium (PDB code: 4AC0). The red residues are the hotspots identified in the DMS study Leander et al. (2020). (B) Four possible conformations of a two-domain TetR molecule with their corresponding free energies (*G*). *G* of the L_I D_I state is set to 0. Blue/green circle (square) denotes the inactive (active) state of LBD/DBD. (C) A simple repression scheme of TetR function. Binding of the ligand (inducer) favors the inactive state of DBD in TetR, which then releases the DNA operator and enables the transcription of the downstream gene. (D) Schematic free energy diagram of the possible binding states of TetR at fixed ligand and operator concentrations. Red, orange and purple arrows show how a mutation can disrupt allostery by 1. increasing ε_L; 2. decreasing ε_D and 3. decreasing y. The L-L_A D_A state is not explicitly shown in the last column as the doubly-bound L-L_A D_A -D state is expected to have a lower free energy. Note that mutations that change the binding affinities of the active LBD/DBD to ligand/operator are not discussed here as we focus on the intrinsic allosteric properties of the TF itself.

Residue number	Distance to DNA operator (Å)	Distance to ligand (Å)
26	7.3	24.7
32	12.6	30.4
42	8.1	25.0
44	9.4	21.6
47	7.7	21.9
49	11.4	17.8
53	17.0	12.1
57	22.5	7.0
76	45.7	17.9
98	19.9	15.6
102	18.1	14.2
105	24.8	7.7
132	39.3	16.0
143	29.4	16.9
146	25.8	17.6
147	26.8	16.0
150	23.2	19.0
174	34.5	14.9
176	38.8	19.5
177	35.5	17.5
203	55.1	28.7

Figure 3—figure supplement 9. The distances presented in the table are estimated using the crystal structure of TetR (PDB ID: 4AC0). Details about the distance calculations are presented in our previous work ***Leander et al.*** (***2022***).

Table 1.

Distances to the DNA operator and ligand of the 21 residues under mutational study.

Mutant	ϵ_L^1	ϵ_L^2	γ^1	γ^2
WT	$6.61^{6.73}_{6.51}$	$6.62^{6.73}_{6.51}$	$5.29^{5.38}_{5.20}$	$5.29^{5.38}_{5.20}$
Q32A-E147G	$7.29^{7.53}_{7.02}$	$7.27^{7.53}_{7.02}$	$2.45^{2.52}_{2.38}$	$2.45^{2.52}_{2.38}$
R49G	$8.62^{8.84}_{8.40}$	$8.62^{8.85}_{8.42}$	$1.66^{1.72}_{1.60}$	$1.65^{1.71}_{1.59}$
D53H	$5.46^{5.80}_{5.09}$	$5.46^{5.79}_{5.05}$	$1.62^{1.66}_{1.57}$	$1.62^{1.67}_{1.57}$
P105M	$7.23^{7.77}_{6.70}$	$7.24^{7.76}_{6.59}$	$0.92^{0.98}_{0.86}$	$0.92^{0.98}_{0.86}$
Y132A	$2.35^{2.55}_{2.15}$	$2.36^{2.55}_{2.17}$	$6.23^{6.54}_{5.97}$	$6.22^{6.55}_{5.96}$
G143M	$6.92^{7.18}_{6.67}$	$6.91^{7.15}_{6.68}$	$1.52^{1.56}_{1.47}$	$1.52^{1.56}_{1.47}$
E150Y	$6.39^{6.73}_{6.01}$	$6.38^{6.73}_{5.99}$	$1.72^{1.79}_{1.66}$	$1.72^{1.78}_{1.66}$
PIF	$11.05^{11.17}_{10.92}$	$11.05^{11.18}_{10.90}$	$1.54^{1.59}_{1.49}$	$1.54^{1.59}_{1.49}$
C203V	$4.51^{4.74}_{4.27}$	$4.53^{4.78}_{4.27}$	$6.95^{10.23}_{5.89}$	$7.47^{15.84}_{6.01}$
G102D-T26A	$7.23^{7.36}_{7.09}$	$7.22^{7.35}_{7.11}$	$4.31^{4.51}_{4.16}$	$4.31^{4.52}_{4.15}$
G102D-Y42M-I57N	$8.21^{8.34}_{8.09}$	$8.21^{8.34}_{8.09}$	$2.83^{2.89}_{2.78}$	$2.83^{2.88}_{2.78}$
G102D-K98Q	$5.96^{6.36}_{5.51}$	$5.97^{6.37}_{5.55}$	$2.14^{2.28}_{2.01}$	$2.14^{2.29}_{2.00}$
G102D-L146A	$5.70^{5.88}_{5.51}$	$5.70^{5.88}_{5.52}$	$5.43^{6.05}_{5.03}$	$5.42^{6.05}_{5.03}$
G102D-HQQ	$7.56^{7.83}_{7.30}$	$7.57^{7.86}_{7.23}$	$1.54^{1.61}_{1.48}$	$1.54^{1.60}_{1.48}$
Y132A-G102D-T26A	$9.55^{10.25}_{8.77}$	$9.67^{10.51}_{8.92}$	$-2.96^{-2.58}_{-3.39}$	$-3.02^{-2.66}_{-3.47}$
Y132A-R49G	$5.77^{5.98}_{5.56}$	$5.78^{5.98}_{5.58}$	$3.11^{3.16}_{3.05}$	$3.11^{3.16}_{3.05}$
Y132A-PIF	$8.71^{8.93}_{8.48}$	$8.70^{8.93}_{8.47}$	$3.69^{3.84}_{3.57}$	$3.69^{3.83}_{3.57}$
Y132A-C203V	$4.14^{4.32}_{3.94}$	$4.15^{4.34}_{3.96}$	$7.82^{11.12}_{6.46}$	$9.30^{16.72}_{6.76}$
C203V-R49G	$5.40^{5.63}_{5.14}$	$5.39^{5.66}_{5.13}$	$2.38^{2.43}_{2.33}$	$2.38^{2.44}_{2.33}$
C203V-D53H	$5.26^{5.53}_{4.98}$	$5.26^{5.51}_{4.97}$	$1.42^{1.46}_{1.39}$	$1.43^{1.46}_{1.39}$
C203V-G102D-L146A	$3.13^{3.43}_{2.81}$	$3.16^{3.49}_{2.78}$	$6.74^{9.01}_{6.00}$	$6.99^{13.63}_{6.03}$
C203V-PIF	$8.30^{8.61}_{7.95}$	$8.30^{8.65}_{7.94}$	$3.49^{3.64}_{3.36}$	$3.49^{3.64}_{3.35}$

Figure 3—figure supplement 10. The column of p^1/p^2 shows the Bayesian inference results using the Gaussian prior distribution of γ centered at 5 k_BT with a standard deviation of 2.5/5 k_BT (p=ϵ_L or γ). The numbers in the table are the medians of the inferred posterior distributions for the corresponding parameters, with their superscripts/subscripts labeling the upper/lower bound of the 95% credible regions.

Table 2.

Bayesian inference results with different prior distributions of γ.

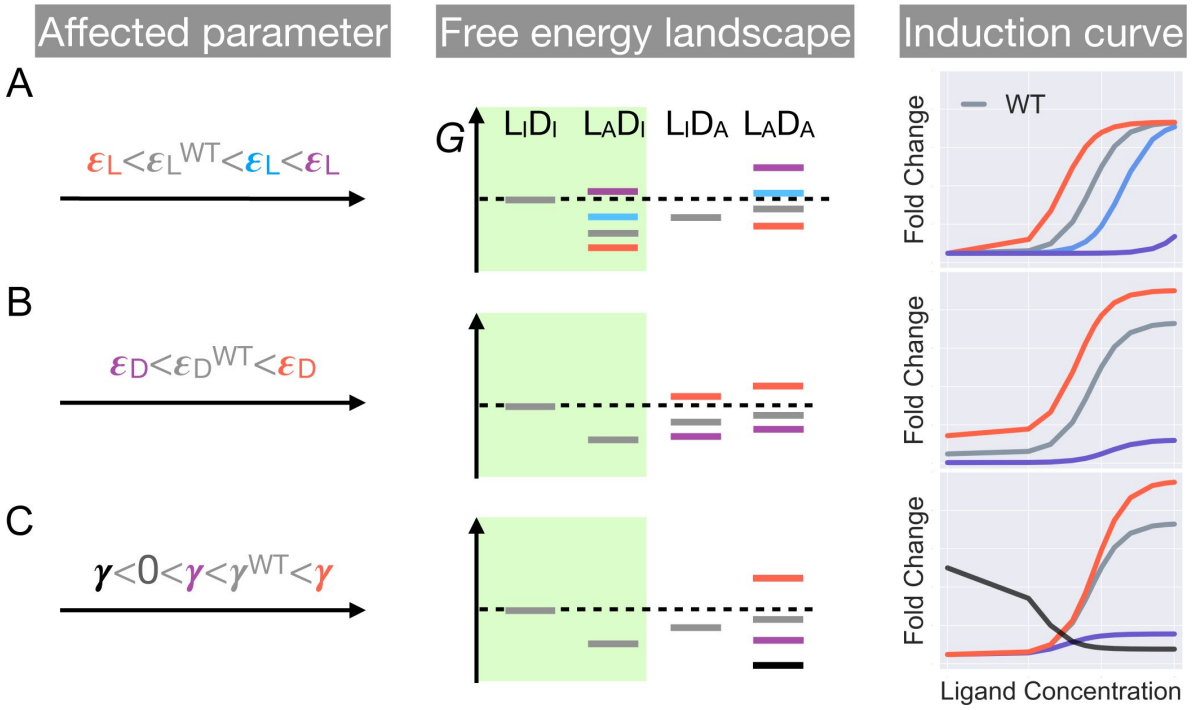

Figure 2.

Schematic illustration of the characteristic effects of perturbations in the three biophysical parameters on the free energy landscape and the corresponding induction curves of a two-domain allosteric system. Panels A, B and C illustrate how changing ε_L, ε_D, and γ alone affects the free energy landscape for the binding states shown in ***Figure 1*** D and the induction curve. For the black induction curve in (C), the values of ε_L and ε_D are also adjusted to aid visualization of the negative monotonicity of the gene expression level (fold change) as a function of ligand concentration. The green shade in the middle column separates the DNA-bound states from the rest. In the free energy landscapes shown in the middle column, ligand- or DNA-binding is always assumed when the corresponding domain is in the active conformation.

Figure 2—figure supplement 1. Statistical weights of promoter occupancy states and repressor states.

Figure 2—figure supplement 2. Equilibria among different conformational and binding states of the repressor.

Figure 2—figure supplement 3. Extended parametric study of main text ***Equation 1***.

of a dead mutation depends on which biophysical parameters it perturbs and by how much. At a qualitative level, the distributed nature of dead and rescuing mutations observed in the DMS measurement emerges naturally from the two-domain model Leander et al. (2020).

In summary, the interplay of intra- and inter-domain properties that govern the free energy landscape of TetR's conformational and binding states, as elucidated by the two-domain model, aligns well with the unexpected DMS results on a qualitative level. To gain deeper insight into TetR allostery and the model itself, we aim to establish a quantitative framework with the model that accurately captures mutant induction curves in the next section.

System-level ramifications of the two-domain model

The discussions in the previous section and ***Figure 1*** are primarily meant to give an intuitive and qualitative understanding of the two-domain model and rationalization of recent DMS measurements Leander et al. (2020, 2022). In this section, we further establish a quantitative connection between the model and the induction curves of TetR variants, leveraging the recent success of linking sequence-level perturbations to system-level responses Daber et al. (2011); Chure et al. (2019); Garcia and Phillips (2011); Brewster et al. (2014); Weinert et al. (2014); Rydenfelt et al. (2014); Razo-Mejia et al. (2017). An induction curve describes the in vivo expression level of the TetR-regulated gene as a function of inducer concentration.

As described in the last section, the intra-domain parameters (ε_D, ε_L) and inter-domain parameter (γ) of the two-domain model collectively determine the free energy landscape of TetR (***Figure 1***). Consequently, a degenerate relationship arises between combinations of parameter values and the induction level at a specific ligand concentration as measured in the DMS study. To tease apart the allosteric effects of different parameters, we aim to formulate their connection to the full induction curve, which is characterized by (1) the expression level of the TF-regulated gene without ligand (leakiness), (2) gene expression level at saturating ligand concentration (saturation) and (3) the ligand concentration required for half-maximal expression (EC_{50}). As revealed in previous studies, these induction curve properties encode information for the key parameters of an allosteric regulation system, for example, the TF binding affinity to ligand and operator, equilibrium between different conformational states of the TF and the abundance of various essential molecules within the system. The establishment of a quantitative connection between the MWC model and the induction curve has yielded valuable insights into several allosteric systems Eaton (2022); Daber et al. (2011); Chure et al. (2019). However, the analogous aspects within a multi-domain thermodynamic model for allostery require further investigation.

Inspired by the pioneering works on transcription with MWC models Daber et al. (2011); Chure et al. (2019), we derived a quantitative relation between the gene expression level in cells and the three biophysical parameters of the two-domain model (***Equation 1***). Briefly, the ratio of the expression level of a TF-regulated gene to that of an unregulated gene, termed fold change (F C) and bound between 0 and 1, is used to quantify gene expression. The gene expression level on the other hand, is assumed to be proportional to the probability that a promoter in the system is bound by RNA polymerase, p(RNAP). Thus, F C is evaluated as the ratio of p(RNAP) in the presence of the TF to that in the absence of the TF. Intuitively, p(RNAP) can be calculated based on the equilibria among different binding and conformational states of the TF (***Figure 2***—figure Supplement 1 and ***Figure 2***—figure Supplement 2), which are determined by the allosteric properties (ε_D, ε_L and γ) and several other parameters. Therefore, F C can be expressed as a function of these parameters, which under the assumption that intra- and inter-domain energetics adopt typical values of several $k_B T$, is simplified to ***Equation 1***.

$$FC = \left(1 + R^* e^{-\varepsilon_D} \frac{1 + e^{-\varepsilon_L - \gamma}\left(\frac{c}{K}\right)^2}{1 + e^{-\varepsilon_L}\left(\frac{c}{K}\right)^2}\right)^{-1} \quad (1)$$

Here, R^* is the rescaled TF copy number in the cell; c is ligand concentration, and K is the dissociation constant of ligand to the repressor with an active LBD. As we focus on understanding how sequence level perturbations are manifested in the allosteric properties of the protein (depicted by ε_D, ε_L and γ), the residues we choose for mutational study here are mostly not in direct contact with either the ligand or the operator (see supplementary file for more discussions). Thus, K and R^*, which is determined by the TF copy number in the cell and the affinity of the operator to the repressor with an active DBD, are taken to be constants across mutations in all subsequent discussions Chure et al. (2019). Detailed derivations of ***Equation 1*** are provided in the supplementary file.

Despite the considerable degeneracy in the activity (inducible and noninducible) within the parameter space of the two-domain model (***Figure 1*** D), ***Equation 1*** demonstrates that mutations affecting distinct biophysical parameters can be discerned based on their characteristic effects on the induction curve.

First, as ε_L and γ have no effect on the leakiness of the induction curve, only mutations that modify ε_D can lead to its changes (***Figure 2*** and Supplementary file for additional discussions). In addition, these mutations also change the level of saturation (F C value where the induction curve plateaus at large c). Thus, dead mutations that disrupt allostery by decreasing ε_D alone will uniquely feature a noticeably lower leakiness and a lower level of saturation compared with the WT (***Figure 1*** D and ***Figure 2***, see also Supplementary file and ***Figure 2***—figure Supplement 3 for more discussions). Second, mutations that solely perturb the other intra-domain property ε_L, a crucial determinant of TetR's ligand detection limit, primarily shift the EC_{50} of the induction curve (see ***Equation 1***). As ε_L increases/decreases from the WT value, the induction curve is right/left shifted with leakiness and the level of saturation remaining unchanged (see the blue and red curves of ***Figure 2*** A). However, when ε_L further increases, the induction curve loses the sigmoidal shape, with its sharply varying tail region being the characteristic of a dead mutation that disrupts allostery mainly by increasing ε_L (purple curve of ***Figure 2*** A, see Supplementary file and ***Figure 2***—figure Supplement 3 for more discussions).

Finally, in the high concentration limit, ***Equation 1*** converges to a constant value (see Equation 2).

$$\lim_{c\to\infty} FC = (1 + R^* e^{-\varepsilon_D - \gamma})^{-1} \tag{2}$$

Hence, mutations affecting γ alone will tune the saturation of a sigmoidal induction curve, which increases/decreases as γ increases/decreases (see red and purple curves of ***Figure 2*** C). Therefore, in contrast to the two aforementioned scenarios, dead mutations that disrupt allostery through decreasing γ alone will feature a full sigmoidal induction curve with a low level of saturation and unchanged leakiness compared with the WT (with $\gamma > 0$, see the purple curve of ***Figure 2*** C). Furthermore, as γ dictates the inter-domain cooperativity, it thereby controls the sign of the monotonicity of F C as a function of c (see Supplementary file for detailed proof). Specifically, when γ/0, there is negative/positive cooperativity between ligand and operator binding, and F C increases/decreases monotonically with c (see ***Figure 2*** C). When $\gamma = 0$, however, the bindings of ligand and operator become independent of each other, and c no longer affects F C (***Figure 2***—figure Supplement 3).

The distinctive roles of the three biophysical parameter on the induction curve as stipulated in ***Equation 1*** could be understood in an intuitive manner as well. First, the value of ε_D controls the intrinsic strength of binding of TetR to the operator, or the intrinsic difficulty for ligand to induce their separation. Therefore, it controls how tightly the downstream gene is regulated by TetR without ligands (reflected in leakiness) and affects the performance limit of ligands (reflected in saturation). Second, the value of ε_L controls how favorable ligand binding is in free energy.

When ε_L increases, the binding of ligand at low concentrations become unfavorable, where the ligands cannot effectively bind to TetR to induce its separation from the operator. Therefore, the fold-change as a function of ligand concentration only starts to noticeably increase at higher ligand concentrations, resulting in larger EC_{50}. Third, as discussed above, γ controls the level of anti-cooperativity between the ligand and operator binding of TetR, which is the basis of its allosteric regulation. In other words, γ controls how strongly ligand binding is incompatible with operator binding for TetR, hence it controls the performance limit of ligand (reflected in saturation).

Having identified the distinctive impacts of the different allosteric parameters of the two-domain model on the induction curve, as outlined in ***Equation 1***, we next apply the model to analyze actual experimental induction curves of TetR mutants. The analysis enables us to uncover the underlying biophysical factors contributing to diverse mutational effects. Additionally, it allows us to evaluate the model's validity in capturing TetR allostery by assessing its accuracy in reproducing the experimental data.

Extensive induction curves fitting of TetR mutants

With the diagnostic tools established, we mapped mutants to the parameter space of the two-domain model through fitting of their induction curves. We choose 15 mutants for analysis in this section, which contain mutations that span different regions in the sequence and structure of TetR (***Figure 3***—figure Supplement 1 and ***Figure 3***—figure Supplement 9). Five of the 15 mutants consist of a dead mutation G102D and one of its rescuing mutations (see the third row of ***Figure 3*** A), while the other 10 contains the WT, 8 single mutants and a double mutant Q32A-E147G (see the first two rows of ***Figure 3*** A and Supplementary file section 7 for more discussions). In all cases, fitting of an induction curve is divided into two steps; first, at c = 0, ***Equation 1*** can be rearranged to give which enables the direct calculation of ε_D from the leakiness of the induction curve; second, ε_L and γ are inferred based on the remaining induction data using the method of Bayesian inference Chure et al. (2019). Briefly, given ε_D calculated in the first step, we select a set of ε_L and γ values from physical ranges of the parameters, based on the probability of observing the induction curve with the parameter values using Monte Carlo sampling. The medians of the selected sets of ε_L and γ values, which are known as posterior distributions, are reported as the inferred parameter values, and error bars show the 95% credible regions of the posterior distributions (***Figure 3*** B and ***Figure 4***—figure Supplement 2B). All details are provided in the "*Materials and methods*" section and Supplementary file.

$$\varepsilon_D = -ln\left(\frac{leakiness^{-1} - 1}{R^*}\right), \tag{3}$$

As shown in ***Figure 3*** A, the fitted curves accurately capture the induction data of all the mutants studied here, enabling the quantification of their biophysical parameters with little uncertainty (see ***Figure 3*** B and ***Figure 3***—figure Supplement 10). These results support the general applicability of the two-domain model to describing TetR allostery, as these 15 mutants vary significantly in terms of location of mutations and phenotype. They are one to four mutations away from the WT, and the sites of mutations are distributed across LBD, DBD and the domain interface (***Figure 3***—figure Supplement 1). In terms of the phenotype, they fall into different classes as characterized by the F C value at c = 1000 nM (F C^{1000}), including dead (F C^{1000} < 0.1), enhanced induction (F C^{1000} > F C^{1000}) and neutral activity (the rest).

Besides inspecting the goodness of fit, a closer examination of the induction curves and the Bayesian inference results reveal additional features of the two-domain model of TetR allostery. First, the apparent binding affinity of TetR to the ligand (anhydrotetracycline; aTC) and operator (*tet02*) used in our experiments are estimated to be about 17.4 k_B T and 16.4 k_B T, respectively, based on the parameter values inferred for the WT (see Supplementary file for detailed

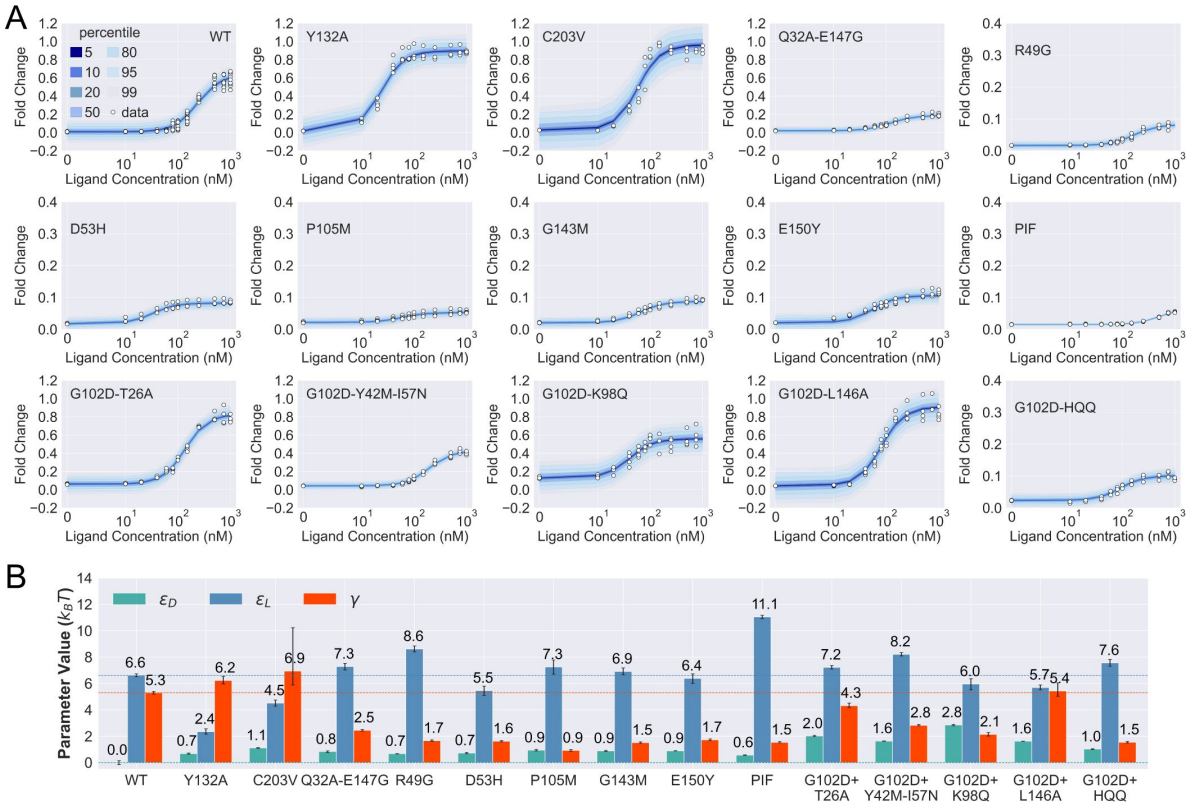

Figure 3.

Induction data of 15 TetR mutants and the corresponding parameter estimation results. (A) Shaded blue curves in each plot show the percentiles of the simulated fold-change measurements using the inferred posterior parameters of the mutant. The white data points represent the corresponding experimental induction measurement of 4 or more biological replicates (three replicates for C203V and G102D-HQQ). (B) The inferred parameter values of the 15 mutants. The error bars of ε_L and γ represent the 95thpercentile of the Bayesian posterior samples, while the error bar of ε_D is calculated based on the standard error of the mean (SEM) of the corresponding leakiness measurement. The horizontal lines indicate the WT parameter values for reference.

Figure 3—figure supplement 1. Sequence and structural distributions of the 21 residues chosen for the mutation analyses in this work.

Figure 3—figure supplement 2. Prior probability distributions and prior predictive check.

Figure 3—figure supplement 3. Distributions of the prior predictive parameters and the corresponding posterior distributions.

Figure 3—figure supplement 4. Distributions of rank statistics of the prior predictive parameters relative to the corresponding posterior samples.

Figure 3—figure supplement 5. Sensitivity analysis for model parameter inference.

Figure 3—figure supplement 6. Posterior predictive check of mutant G102D-Y42M-I57N.

Figure 3—figure supplement 7. Theoretical induction curves of R49G, D53H, P105M and G143M with WT γ value.

Figure 3—figure supplement 8. Sorting scheme to identify dead variants.

Figure 3—figure supplement 9. Distances to the DNA operator and ligand of the 21 residues under mutational study.

Figure 3—figure supplement 10. Bayesian inference results with different prior distributions of γ.

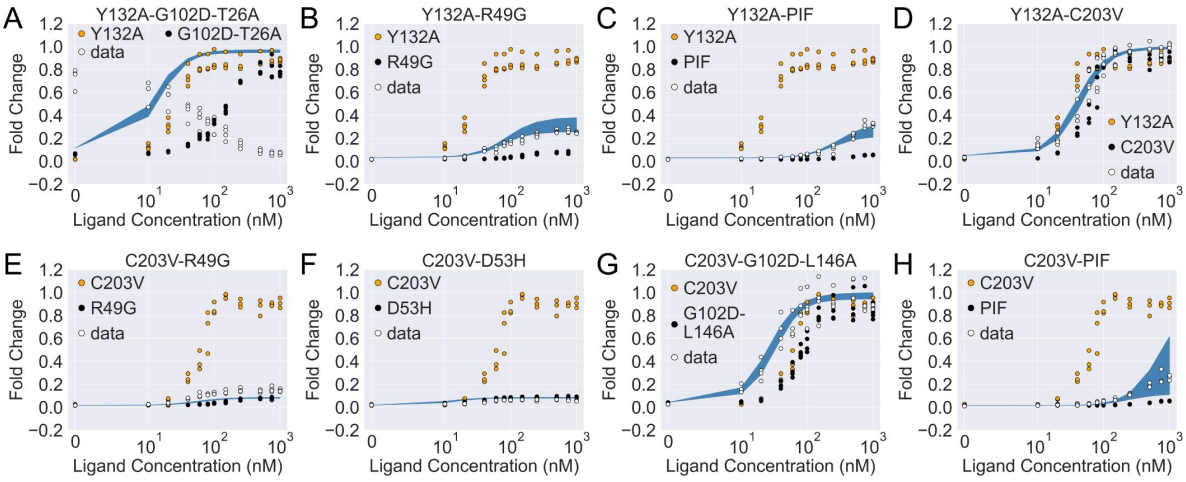

Figure 4.

The induction curves for the eight combined TetR mutants from experimental measurement and prediction from the modified additive model. In each plot, black, orange and white points represent the experimental data for mutant 1, mutant 2 and the combined mutant (named mutant 1-mutant 2), specified in the legend and title. The blue band show the 95thpercentile of the indu{ ction curve prediction from th} e modified additive model. The modification to the basic additive model in each plot is specified by the 6 weights {1,ε_D , $^{\alpha}$2,ε_D , $^{\alpha}$1,ε_L , $^{\alpha}$2,ε_L , $^{\alpha}$1,γ , $^{\alpha}$2,γ (see ***Equation 4***), which are (A) {1, 1, 1, 1, 1, 1}; (B) {1, 1, 0.5, 1, 1, 1}; (C) {1, 1, 0.5, 1, 1, 1}; (D) {1, 1, 0, 1, 1, 1}; (E) {0, 1, 1, 1, 0, 1}; (F) {0, 1, 1, 1, 0, 1}; (G) {0, 1, 1, 1, 1, 1}; (H) {0, 1, 1, 1, 1, 1}.

Figure 4—figure supplement 1. The induction curves of the eight combined mutants calculated using the basic additive model.

Figure 4—figure supplement 2. Induction curves of the eight combined mutants and the corresponding parameter estimation results as well as the basic additive model predictions.

calculations); these agree well with the range of reported experimental values Scholz et al. (2000); Schubert et al. (2004); Kędracka-Krok and Wasylewski (1999); Kamionka et al. (2004); Bolintineanu et al. (2014); Normanno et al. (2015). Second, as shown in ***Figure 3*** B, the perturbations in ε_D are generally small in magnitude (< 1 k_BT) among the dead mutants, while substantially larger perturbations (up to ~ 5 k_BT) are observed for ε_L and γ. The latter observation is in line with the predictions of the model (see the previous section) that two types of qualitatively different induction curves are expected for partially dead mutants (see the first and second rows of ***Figure 3*** A). Specifically, the induction curve of P176N-I174K-F177S (PIF) loses the sigmoidal shape, with its sharply varying tail region suggesting a significant increase of ε_L. This is confirmed by the parameter fitting result, which shows that the triple mutations of PIF, located in the core region of LBD (Supplementary file and ***Figure 3*** —figure Supplement 1), lead to the largest increase of ε_L among all mutants (4.5 k_BT higher than the WT, see ***Figure 3*** B). The induction curves of the other four dead mutants (R49G, D53H, P105M and G143M), however, maintain the sigmoidal shape yet with low levels of saturation. As they all exhibit a higher ε_D (leakiness) than the WT, the low levels of saturation have to result solely from weakened inter-domain couplings (***Figure 3***). In other words, these four dead mutations, located mostly at the domain interface (***Figure 3*** —figure Supplement 1), disrupt allostery primarily through decreasing γ. Indeed, when the γ of these mutants is set to the WT value but keeping their respective ε_D and ε_L parameters unchanged, higher F C^{1000} values than the WT are obtained instead (***Figure 3*** —figure Supplement 7).

Despite the discussion of two limiting types of changes in the induction curves, it is interesting to observe in ***Figure 3*** B that the three biophysical parameters, especially ε_L and γ, are often perturbed together in the mutants. Indeed, although the three parameters are theoretically independent of each other, at the structural level, it is less likely to have a scenario where a mutation perturbs inter-domain coupling (γ) but leaves intra-domain properties unchanged. Lastly, while quantification of G102D from its flat induction curve incurs large uncertainties, (***Figure 2*** —figure Supplement 3), the diversities of the induction curves and the biophysical parameters of the G102D-rescuing mutants (***Figure 3*** B) provide clear support for the qualitative anticipation from the previous section; i.e., rescuing mutations of a dead mutant may restore inducibility through different combinations of tuning ε_D, ε_L and γ. For example, while Y42M-I57N and K98Q both rescue G102D to achieve similar F C^{1000}, they exert distinct influences on ε_D and ε_L, as reflected in the variations of leakiness and EC_{50} between the corresponding induction curves. In another case, while the induction curves of G102D-T26A and G102D-L146A show comparable values of saturation and leakiness, their different EC_{50} values suggest the different effects of the two rescuing mutations on ε_L, further quantified by the inferred parameter values. The diverse mechanistic origins of the rescuing mutations revealed here provide a rational basis for the broad distributions of such mutations. Integrating such thermodynamic analysis with structural and dynamic assessment of allosteric proteins for efficient and quantitative rescuing mutation design could present an interesting avenue for future research, particularly in the context of biomedical applications Pan et al. (2005); Liu and Nussinov (2008).

In summary, ***Equation 1*** accurately captures the induction curves of a comprehensive set of TetR mutants using a minimum set of parameters with realistic values (see the section "Discussion" and ***Figure 3*** —figure Supplement 1). The two-domain model thus provides a quantitative platform for investigating TetR allostery beyond an intuitive rationalization of the DMS results.

Exploring epistasis between mutations

With the 15 mutants mapped to the parameter space of the two-domain model, we now explore the epistatic interactions between the relevant mutations. To do so, we start by assuming additivity in the perturbation of all three biophysical parameters (see ***Equation 4*** and ***Equation 5***, where p represents any one of ε_D, ε_L and γ).

$$p^{mut1+mut2} - p^{WT} = \alpha_{1,p}\delta p^{mut1} + \alpha_{2,p}\delta p^{mut2} \quad (4)$$

$$\delta p^{mut1} = p^{mut1} - p^{WT} \quad (5)$$

We then evaluate how the induction curves generated by this additive model ($\alpha_{1,p} = \alpha_{2,p} = 1$) deviate from the corresponding experimental results, and the magnitude of deviation quantifies the significance of epistasis. Eight mutation combinations were chosen for the analysis, where we pair up C203V and Y132A, the two single mutations that enhance the level of induction relative to the WT, with mutations from different structural regions of TetR (see Supplementary file section 7 for more discussions).

Although predictions from the additive model are qualitatively correct for 5 of the 8 mutation combinations on phenotypic effects, none of them captures the corresponding induction curve accurately (***Figure 4***—figure Supplement 1). This again highlights the parameter space degeneracy of the phenotypes, and that mechanistic specificity is required of a model for making reliable predictions on combined mutants Li and Lehner (2020). For a deeper understanding of epistatic interactions between the mutations queried here, we next directly fit for the three biophysical parameters of the combined mutants using their induction curves, which are then compared with those obtained from the additive model.

As shown in ***Figure 4***—figure Supplement 2A, the induction data of all eight combined mutants are well captured by the fitted curves, which reaffirms the applicability of the two-domain model. Interestingly, despite the discrepancy between the experimental induction curves and those predicted by the additive model, the fitted parameters of the combined mutants are comparable to those from the additive model in many cases (see ***Figure 4***—figure Supplement 2B). In this regard, one noticeable example is the mutant C203V-G102D-L146A, for which the result of direct fitting is close to the additive model in terms of both ε_L and γ (with a difference of $\leqslant 0.5\ k_B T$), while they differ more in ε_D ($1.6\ k_B T$). Inspired by such observations, we then seek the minimal modifications to the additive model that can account for epistasis. As C203 is one of the most distant residues from DBD in TetR, we reason that its effect on ε_D may get dominated by mutations much closer to the DNA binding residues like G102D and L146A (***Figure 3***—figure Supplement 1 and ***Figure 3***—figure Supplement 9). Remarkably, when we quench C203V's contribution to ε_D in the additive model of C203V-G102D-L146A ($\alpha_{C203V,\varepsilon} = 0$, see ***Equation 4***), the predicted induction curve well recapitulates the experimental data (***Figure 4*** *G*). In another example, when C203V is combined with the triple mutations PIF, which are much closer to the DBD, the fitted parameters of the combined mutant also align well with the additive model except only for ε_D. Here, quenching C203V's contribution to ε_D again leads to good agreement between the additive model and experiment in terms of the induction curve (***Figure 4*** H).

The epistatic effects in other C203V-containing combined mutants can be largely accounted for by modifying the additive model following the same physical reasoning as above. For instance, mutation D53H is near the DNA-binding residues and located at the domain interface, which suggests its dominant role in defining the DBD energetics and inter-domain cooperativity when paired up with C203V Scholz et al. (2004). Accordingly, quenching C203V's effect on both ε_D and γ in the additive model for mutant C203V-D53H leads to dramatic improvement in the induction curve prediction (***Figure 4***—figure Supplement 1F and ***Figure 4*** F). Along this line, success is

also observed when accounting for the epistasis between C203V and R49G by the same approach (***Figure 4*** E). These examples might also explain why C203V, although being able to enhance the induction of TetR, fails to rescue a range of dead mutations including R49A, D53V, G102D, N129D and G196D Leander et al. (2020). More broadly, these observations together indicate that epistasis in combined mutants (e.g., those containing C203V) can be captured by the additive two-domain model with modifications based on physical reasoning.

The epistasis in combined mutants containing Y132A can be understood in a similar manner. Noticeably, the fitted parameter values of Y132A-C203V agree very well with the additive model for ε_D and γ (within a difference of 0.4 $k_B T$), while they differ in ε_L by 3.8 $k_B T$. Interestingly, such discrepancy in ε_L values can be essentially resolved by quenching Y132A's contribution in the additive model (reduced to 0.4 $k_B T$). This likely suggests that the effect of Y132A on ε_L tends to be compromised when combined with other mutations that perturb ε_L. Indeed, for most of the Y132A containing mutants investigated here (Y132A-C203V/PIF/R49G), the accuracy of induction curve prediction by the additive model improves greatly when $\alpha_{Y132A,\varepsilon}$ is tuned down (***Figure 4*** B – D, see Supplementary file for more discussions).

The only exception to this trend is the mutant Y132A-G102D-T26A, for which we observe strong epistasis between Y132A and the dead-rescue mutation pair G102D-T26A. Although both mutations Y132A and G102D-T26A enhance the allosteric response of TetR (***Figure 3***), their combined effects radically change the sign of cooperativity between the two domains (γ), turning the ligand (aTC) from an inducer into a corepressor (***Figure 4*** A and ***Figure 4***—figure Supplement 2B). Here, large disparity exists between the additive model and the direct fitting result in all three biophysical parameters, which cannot be explained by simple modifications of the additive model.

Discussion

Allostery, a major regulatory mechanism in biology, has attracted intense research interest in the past few decades due to its complexity and implications in biomedicine and protein engineering. A central goal is to develop a quantitative understanding of the phenomena through a physical model that can be tested by comprehensive data. Along this line, one of us has in recent years advanced a function-centric approach to studying protein allostery with DMS, which provides a comprehensive and most direct test of our mechanistic understandings. Specifically, we have shown in an unbiased way that allostery hotspots and dead-rescue mutation pairs in four TetR family TFs are distributed across the protein structures Leander et al. (2020, 2022). This highlights that modifying the propagation of conformational distortions between the effector and active sites is not the only way to tune allosteric regulation Leander et al. (2020).

The rich and surprising observations for the TetR family TFs call for a physical understanding of the underlying allostery mechanism, for which we resort to statistical thermodynamic models. Statistical thermodynamic models have played a central role in shaping our understanding of allostery Bacon (1965); Koshland Jr et al. (1966). In particular, Chure et al. have developed the methodology of fitting the MWC model to the induction data of LacI repressors using Bayesian inference Chure et al. (2019). This established the connection between sequence-level perturbations to system-level responses, which enables the exploration of mutational effects on transcription within the framework of biophysical models. However, as pointed out in several previous studies, the MWC model is not consistent with the observation that effector-bound TetR crystal structures are closer to the DNA-bound form compared to the apo crystal structures Motlagh et al. (2014); Reichheld et al. (2009); Hilser et al. (2012). Hence, it's at least difficult to provide a complete picture of TetR allostery with the MWC model. The ensemble allosteric model (EAM) on the other hand, presents a more flexible and detailed domain-specific view of allostery, which can be applied to more complex allosteric systems (e.g., allostery with intrinsically disordered proteins) Motlagh et al. (2014); Hilser et al. (2012).

Inspired by these pioneering developments and our DMS results, in this work, we propose a two-domain statistical thermodynamic model, the parameter-activity degeneracy of which readily elucidates the distributed allosteric network observed in the DMS result of TetR (***Figure 1***). On the other hand, the functional form derived in ***Equation 1*** establishes the qualitative differences in the impacts of various model parameters on the characteristics of the induction curve (***Figure 2***); for example, dead mutations perturbing inter- and intra-domain properties are predicted to cause induction curves with and without a saturating plateau, which are both observed experimentally (***Figure 3***). Moreover, ***Equation 1*** accurately captures the induction data of a diverse set of TetR mutants (***Figure 3***, ***Figure 3***—figure Supplement 1 and ***Figure 4***—figure Supplement 2) in a quantitative manner, enabling their mapping to the model parameter space with high precision. It's noted that the homodimeric nature of TetR is ignored in the current two-domain model to minimize the number of parameters, and additional experimental data could necessitate a more complex model for TetR allostery in the future (see Supplementary file section 8 for more discussions).

The success of ***Equation 1*** allows for a quantitative investigation of epistasis between the characterized mutations. In a previous study of another TF, LacI, using the MWC model, no epistasis was observed between mutations of ligand-binding and DNA-binding residues analyzed therein Chure et al. (2019). In the present analysis of TetR, epistasis is observed in all eight queried mutation combinations, which can be largely rationalized through physical reasoning. For example, our results intuitively indicate that the effect of a distant mutation like C203V on DBD energetics and inter-domain coupling tend to be dominated by mutations much closer to these regions (**Figure 4** and ***Figure 4***—figure Supplement 1). Such phenomena suggest that these mutations affect allosteric regulation by influencing not only the relative populations of conformations in different ligation states, but also through shifting the dominant conformations themselves Zhang et al. (2020). On the other hand, epistasis involving Y132A is more complex. For instance, we observe that Y132A's influence on ε_L is diminished when paired up with other mutations in most cases. Further mechanistic understanding, likely from a biochemical perspective, is required to fully explain this phenomenon. Nonetheless, these observations provide a plausible explanation for why C203V and Y132A, although being able to enhance the induction response of TetR individually, could not rescue a range of dead mutations Leander et al. (2020).

Our results reveal additional insights into the nature of two-domain allostery as well. Although our model assumes no a *priori* correlation between the intra- and inter-domain properties of the TF, we find that they are always modified together by mutations (***Figure 3*** and ***Figure 4***—figure Supplement 2). This immediately points to the interconnectivity of allosteric networks Takeuchi et al. (2019); Reichheld et al. (2009); Scholz et al. (2004). That is, when a residue is involved in the conformational rearrangements induced by both effector and operator binding, it functions as a bridge through which the two events are coupled. Within such a conceptual framework, it is highly unlikely to observe a mutation that changes γ alone without perturbing the intra-domain energetics.

This point is explicitly illustrated in ***Figure 5***, which summarizes the locations of all the characterized 23 mutants in the two-dimensional space of ε_L and γ. Here, the color of the contour plot encodes the F C^{1000} value calculated for each (ε_L, γ) combination together with the WT ε_D value, while the color of the specific mutant data points is based on the true F C^{1000} value. Thus, the color of a data point reflects the ε_D of the corresponding mutant relative to the WT; i.e., a brighter/darker color than the surrounding indicates that the mutant features a higher/lower ε_D value than the WT. Since the variations of ε_D among the investigated mutants are modest compared with ε_L and γ (see ***Figure 3*** B), we'll primarily focus on the latter two in the discussion. Evidently, mutants with the strongest allosteric responses feature small ε_L and large γ, which correspond to the upper left region of ***Figure 5***. Additional mutations in the background of these mutants lead to weaker allosteric response, moving the mutants to the darker regions of the plot. The interconnected nature of allosteric networks described by the two-domain model, however,

dictates that such shifts would take place along the diagonal of the ε_L -γ plane, which describe mutations that modify intra- and inter-domain properties simultaneously. This feature potentially offers a functional advantage of preventing mutants from regions of low allosteric response (corresponding to upper right and lower left of ***Figure 5***), facilitating efficient adaptation to new effectors during evolution. In the future, it is of interest to examine whether such a negative correlation between ε_L and γ is a generic feature of two-domain allostery.

Our results establish the two-domain model as a flexible and quantitative platform for investigating TetR allostery, adding to the value of statistical thermodynamic models as advocated by the seminal works on MWC molecules Daber et al. (2011); Chure et al. (2019). We note, however, that the two-domain model is a more generic description of allostery compared with the MWC model.

First, although our model identifies the importance of intra-domain energetics in tuning the free energies of different TF states, it points out the more fundamental role of inter-domain coupling in defining allosteric response (***Figure 2*** and Supplementary file). A large inter-domain coupling is assumed to be obligatory in the MWC model and required to create the two pre-existing conformations of different ligand and operator affinities in the first place. Various experimental studies as well as our own data reveal that the inter-domain coupling of TetR is amenable to tuning, especially by mutations of residues at the domain interface Reichheld et al. (2009); Scholz et al. (2004); Müller et al. (1995); Hecht et al. (1993). In some cases, even single mutations can reverse the sign of cooperativity between LBD and DBD, indicating that the dead mutational effects observed in the DMS experiments and elsewhere could well originate from diminishing γ. These considerations necessitate an explicit treatment of γ in a physical model of TetR allostery.

Second, the MWC model, when applied to two-domain systems, contains at least four biophysical parameters Daber et al. (2011); Chure et al. (2019), is thus more complex than our two-domain model, which requires only three. The simplicity of our model reduces its parameter space degeneracy, enabling high precision in fitting while being able to accurately describe a broad set of induction data. The three parameters also offer an interpretable mechanistic picture of TetR allostery in a physically transparent fashion.

We have focused our experimental and theoretical analyses on the TetR-family TFs, which represent important systems for building allosteric models, due to their broad involvement in many aspects of cell physiology Ramos et al. (2005); Cuthbertson and Nodwell (2013). Along this line, a natural extension of the current study is to use the two-domain model as a platform for comparing allostery in different TetR homologs Leander et al. (2022). For example, coupling the model with systematic dose-response study of hotspot mutations could reveal the roles of different allosteric hotspots (whether they dictate intra- or inter-domain properties or both). The similarity in key structural features among TetR homologs then enables the comparison of the nature of hotspots at similar structural locations. This could potentially lead to novel insights into the different roles that sequence and structure play in defining the allostery of a system, which is a fundamental question to address in rational engineering of allosteric proteins.

Although our two-domain model is inspired by and established with the data of TetR family TFs, the mechanistic and modelling insights gained here should be generally applicable to other allosteric systems sharing the two-domain architecture. This includes other transcription factors like catabolite activator protein (CAP), a homodimeric TF with a cyclic AMP (effector) binding domain and a DNA binding domain Tzeng and Kalodimos (2012); receptors like pentameric ligand-gated ion channels (pLGICs), which allosterically translate the binding of neurotransmitters to their extra-cellular domains into the activation of ionotropic pores located in their transmembrane domains Sauguet et al. (2015); Hu et al. (2020); and allosteric enzymes like aspartate transcarbamoylase (AT-Case), in which binding of effector like ATP to the regulatory

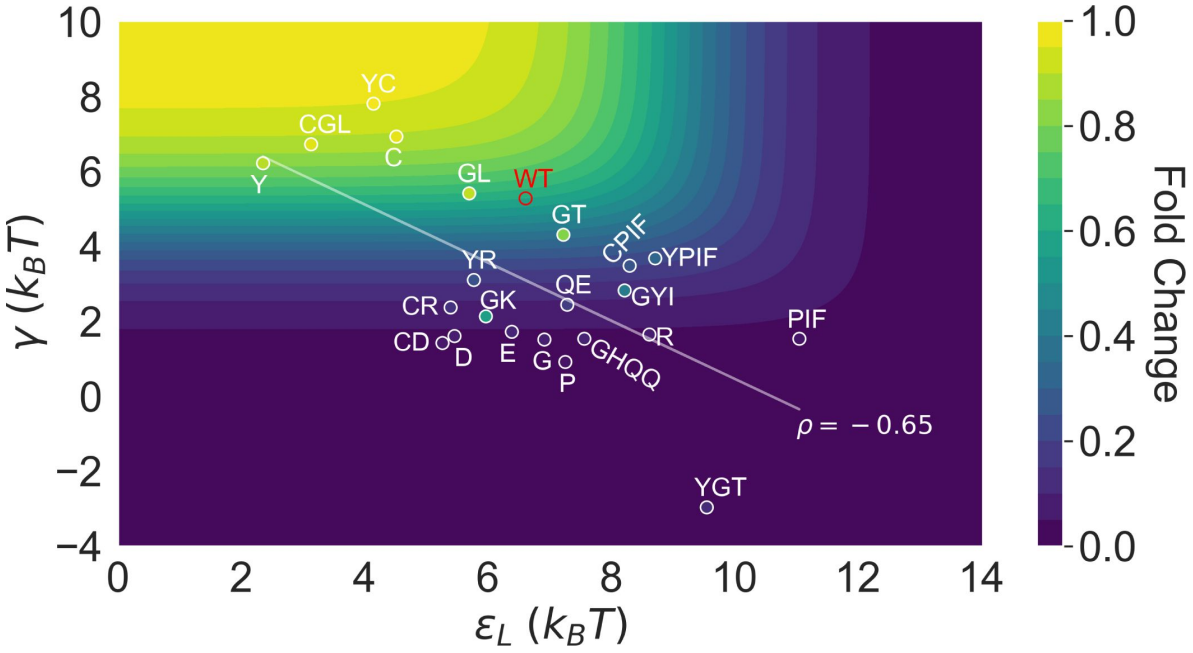

Figure 5.

Distribution of the 23 investigated TetR mutants in the parameter space of the two-domain model illustrates the correlation between perturbations in ε_L and γ. Color of the contour plot encodes the fold change at c = 1000 nM calculated for each point in the two-dimensional space of ε_L and γ with the WT ε_D value. The color within the data point of each mutant is based on the F C^{1000} calculated with its specific ε_D value. The notation of each mutant is abbreviated based on the 1-letter codes of the residues that are mutated. The specific mutations corresponding to each letter code from upper left to lower right are C: C203V; Y: Y132A; GL: G102D-L146A; GT: G102D-T26A; R: R49G; D: D53H; GK: G102D-K98Q; E: E150Y; QE: Q32A-E147G; G: G143M; P: P105M; GYI: G102D-Y42M-I57N; GHQQ: G102D-H44F-Q47S-Q76K; PIF: P176N-I174K-F177S. The least-squares regression line between ε_L and γ is shown with their Pearson correlation coefficient (ρ).

domain allosterically alters the catalytic activity of the functional domain Velyvis et al. (2007); Lipscomb and Kantrowitz (2012). Ultimately, we envision that such model provides a minimalist but physically sound framework for integrating different types of experimental data and computational methods Leander et al. (2022); Yuan et al. (2022); Xie et al. (2022); Tonner et al. (2021) for exploring rational engineering and regulation of allostery for biotechnological and biomedical applications.

Materials and methods

Library construction

Using a low-copy backbone (SC101 origin of replication) carrying spectinomycin resistance, we constructed a sensor plasmid with TetR(B) (Uniprot P04483). The tet*Rb* gene was driven by a variant of promoter apFAB61 and Bba_J61132 RBS Kosuri et al. (2013). On a second reporter plasmid, superfolder GFP Pedelacq et al. (2006) was cloned into a high-copy backbone (ColE1 origin of replication) carrying kanamycin resistance. The expression of the superfolder GFP reporter was placed under the control of the ptetO promoter. To control for plasmid copy number, RFP was constitutively expressed with the BBa_J23106 promoter and Plotkin RBS Kosuri et al. (2013) in a divergent orientation to sfGFP.

Library synthesis

A comprehensive single-mutant TetR library was generated by replacing wildtype residues at positions 2–207 of TetR to all other 19 canonical amino acids (3,914 total mutant sequences). Oligonucleotides encoding each single-point mutation were synthesized as single-stranded Oligo Pools from Twist Bioscience and organized into 6 subpools, spanning six segments of the *tetRd* gene, corresponding to residues 2–39, 40–77, 78–115, 116–153, 154–191, and 192–207 of TetR(B) respectively. Additional sequence diversity was observed in the library due to error rates in the synthesis of single-stranded Oligo Pools, leading to the downstream identification of some double and triple mutant TetR variants. Oligo pools were encoded as a concatemer of the forward priming sequence, a BasI restriction site (5'-GGTCTC), six-base upstream constant region, TetR mutant sequence, six-base downstream constant region, a BsaI site (5'-GAGACC), and the reverse priming sequence. Subpools were resuspended in double-distilled water (ddH_2 0) to a final molal concentration of 25 ng/µL and amplified using primers specific to each oligonucleotide subpool with KAPA SYBR FAST qPCR (KAPA Biosystems; 1-ng template). A second PCR amplification was performed with KAPA HiFi (KAPA Biosystems; 1-µL qPCR template, 15 cycles maximum). We amplified corresponding regions of pSC101_TetR_specR with primers that linearized the backbone, added a BsaI restriction site, and removed the replaced wildtype sequence. Vector backbones were further digested with DpnI, BsaI, and Antarctic phosphatase before library assembly.

We assembled mutant libraries by combining the linearized sensor backbone with each oligo subpool at a molar ratio of 1:5 using Golden Gate Assembly Kit (New England Biolabs; 37 ˚C for 5 min and 60 ˚C for 5 min, repeated 30 times). Reactions were dialyzed with water on silica membranes (0.025-µm pores) for 1 h before transformed into DH10B cells (New England Biolabs). Library sizes of at least 100,000 colony-forming units (cfu) were considered successful. DH10B cells containing the reporter pColE1_sfGFP_RFP_kanR were transformed with extracted plasmids to obtain cultures of at least 100,000 cfu. Following co-transformation, the cultures for each subpool were stored as glycerol stocks and kept at -80 ˚C.

Fluorescence-activated cell sorting

The subpool library cultures were seeded from glycerol stocks into 3 mL lysogeny broth (LB) containing 50 µg/mL kanamycin (kan) and 50 µg/mL spectinomycin (spec) and grown for 16 h at 37 ˚C. Each culture was then back-diluted into two wells of a 96-well plate containing LB kan/spec

media using a dilution factor of 1:50 and grown for a period of 5 hours at 37 ˚C. Following incubation, each well containing saturated library culture was diluted 1:75 into 1× phosphate saline buffer (PBS), and fluorescence intensity was measured on a SH800S Cell Sorter (Sony). We first gated cells to remove debris and doublets and selected for variants constitutively expressing RFP. Using this filter, we then proceeded to draw an additional gate to select for mutants that displayed low fluorescence intensities in the absence of anhydrotetracycline (aTC). This gate allowed us to select for mutants which retained the ability to repress GFP expression in the presence of an inducer, using prior measurements of WT TetR(B) as a reference for selecting repression competent mutants Leander et al. (2020). Utilizing these gates, we sorted 500,000 events for each gated population and recovered these cells in 5 mL of LB at 37 ˚C before adding 50 µg/mL of kan and spec. Following the addition of antibiotics, the cultures were incubated at 37 ˚C for 16 hours.

Following overnight growth, each culture was back diluted into two wells of a 96-well plate containing LB kan/spec media using a 1:50 dilution factor. Upon reaching an OD600 ~ 0.2, aTC was added to one of the two wells at a final concentration of 1 µM, with the well not receiving aTC serving as the uninduced control population. Cells were then incubated for another 4-hour growth period at 37 ˚C before being diluted into 1x PBS using a dilution factor of 1:75, and fluorescence intensity was measured on a SH800S Cell Sorter.

We first gated cells to remove debris and doublets and selected for variants constitutively expressing RFP before obtaining the distribution of fluorescence intensities (FITC-A) across the uninduced and induced populations of each of the 6 subpools (***Figure 3***—figure Supplement 8). Using the uninduced control population of each subpool as a reference, gates were drawn to capture mutants which displayed no response to the presence of aTC in the induced populations. Using these gates, 500,000 events were sorted from the induced populations of each subpool and cells were subsequently recovered at 37 ˚C using 5 mL of LB media before being plated onto LB agar plates containing 50 µg/mL kan and spec.

Clonal screening of dead mutants

To screen for functionally deficient variants of TetR, 100 individual colonies were picked from each subpool and grown to saturation in a 96-well plate for 6 hours. Saturated cultures were then diluted 1:50 in LB-kan/spec media and grown in the presence and absence of 1 µM aTC for 6 hours before OD600 and GFP fluorescence (Gain: 40; Excitation: 488/20; Emission: 525/20) were read on a multiplate reader (Synergy HTX, BioTek). Fluorescence was normalized to OD600, and the fold inductions of each clone were calculated by dividing its normalized fluorescence in the presence of inducer by the normalized fluorescence in the absence of inducer. The fold-induction of WT TetR was tested in parallel with these screens to serve as a benchmark for function, and clones which displayed < 50% activity to WT were replated and validated in triplicate before being sent for sanger sequencing (Functional Biosciences).

aTC dose response measurements

TetR mutants identified during clonal screening were reinoculated into 3 mL of LB Kan/Spec media and grown overnight. After an overnight growth period, each culture was added to 4 rows of 12 wells in a 96-well plate containing LB Kan/Spec media using a dilution factor of 1:50. Each mutant was tested across 12 different concentrations of aTC in quadruplicate fashion, with each row having an identical concentration gradient across the 12 wells. The aTC concentration gradient across the 12 wells were 0 nM, 10 nM, 20 nM, 40 nM, 60 nM, 80 nM, 100 nM, 150 nM, 250 nM, 500 nM, 750 nM, and 1µM aTC.

Following reinoculation into 96-well plates, selected mutants were placed on a plate shaker set to 900 RPM and incubated at 37 ˚C for 5 hours. Following this 5-hour growth period, the plates were removed from the plate shaker and the OD600 and GFP fluorescence (Gain: 40; Excitation: 488/20;

Emission: 525/20) of each well was read using a multiplate reader (Synergy HTX, BioTek). Fluorescence was normalized to OD600 for each well. The normalized fluorescence at each concentration was measured for 4 replicates of each mutant (unless otherwise stated). The fluorescence of GFP reporter-only control (no TetR), grown under identical conditions, was measured in the same way. This reporter-only control served as an upper bound to the fluorescence that could be measured in the experiment and was accompanied by a WT TetR-GFP reporter control, used to certify the precision of measurements made at different times.

Synthesis of combined TetR mutants

To assess the predictive capability of the additive model, eight combined mutants were selected to undergo aTC dose response characterization. These combined mutants were synthesized using clonal DNA fragments from Twist Biosciences coding for the amino acid sequence of each of the selected combined mutants. The gene fragments were individually cloned into sensor plasmid backbones identical to those used in the previous identification of non-functional TetR(B) mutants following the manufacturers protocol for Gibson Assembly (New England Biolabs). The newly constructed plasmids carrying each of the combined mutants were then transformed into E. coli (DH10B) cells containing a GFP reporter plasmid identical to that used in the previous characterization of non-functional TetR(B) mutants. After a 1-hour recovery period, 100 µL of recovered cells were plated onto LB kan/spec agar plates for each of the combination mutants and incubated for 16 hours at 37 ˚C.

Following overnight growth, individual colonies were picked and inoculated into 3 mL of LB kan/spec media to be grown overnight at 37 ˚C. Following overnight growth, samples from each culture were submitted for sanger sequencing to confirm the identity of each of the synthesized combined mutants. Following sequence verification, the aTC dose-response behavior of each combined mutant was characterized using an experimental setup consistent with dose-response measurements made for the previously identified TetR(B) mutants.

Model parameter estimation

As described above, the estimation of the three biophysical parameters (ε_D, ε_L and γ) for each mutant is divided into two steps. Firstly, as ε_L and γ do not affect F C at $c = 0$ (***Equation 1***), we directly calculate the value of ε_D from the leakiness of an induction curve, which is measured with high precision in our experiments. With the calculated ε_D ($\varepsilon_D{}^{wT}$ is set to 0 as reference), we then fit the full induction curve to obtain the values of ε_L and γ using the method of Bayesian inference. Here, we first construct the statistical model that describes the data generating process based on ***Equation 1***, and specify the prior distributions of the relevant parameters. This enables the derivation of the conditional probability of the parameter values of a mutant given its induction data, known as the posterior distribution. The posterior distribution is then sampled using Markov chain Monte Carlo (MCMC), from which we infer the values of ε_L and γ directly. The validity of the statistical model and computational algorithm is fully tested with several metrics, and all details regarding the parameter estimation process briefed here are provided in the Supplementary file.

Code and data availability

All code and data used in this work can be accessed at the Github repository *https://github.com/liuzhbu/Two_Domain_Allostery*.

Author contributions

Z.L., S.R. and Q.C. conceptualized the work. Z.L. and T.G. conducted the research. Z.L. and T.G. analyzed the data. All authors are involved in writing the manuscript.

Competing interests

Qiang Cui: Senior editor, *eLife*. The other authors declare that no competing interests exist.

Acknowledgements

This work is funded by NIH Director's New Innovator Award DP2GM132682 (SR) and Shaw Scientist Award (SR), and R35-GM141930 (QC). Development of the Bayesian inference model was partially supported by grant ML-21-016 from the Dreyfus foundation (QC). Computational resources from the Extreme Science and Engineering Discovery Environment (XSEDE), which is supported by NSF grant number ACI-1548562, are greatly appreciated; part of the computational work was performed on the Shared Computing Cluster which is administered by Boston University's Research Computing Services (URL: *https://www.bu.edu/tech/* support/research/).

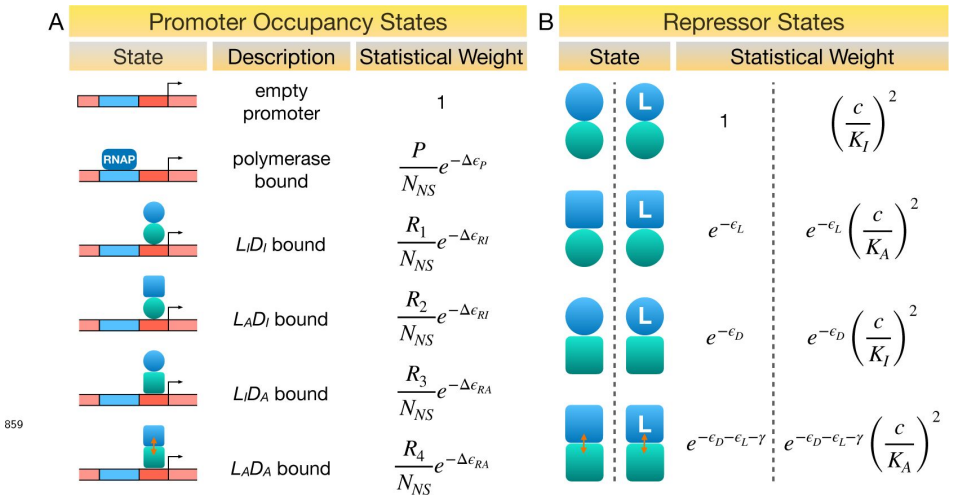

859

Figure 2—figure supplement 1.

Statistical weights of promoter occupancy states and repressor states. (A) Statistical weights of the promoter occupancy states, with the empty promoter state taken as reference. P is the average number of RNAP per cell. R_1, R_2, R_3 and R_4 denote the average number of repressors in the L_I D_I, L_A D_I, L_I D_A and L_A D_A state per cell, respectively. N_{Ns} is the number of non-specific DNA binding sites in the cell. $\Delta\varepsilon_P$, $\Delta\varepsilon_{RA}$ and $\Delta\varepsilon_{RI}$ represent the energy differences between specific and non-specific DNA binding of RNAP, repressor with DBD in the active and inactive conformations, respectively. (B) Statistical weights of the allosteric states of the repressor, with the L_I D_I state taken as reference. K_A and K_I are the dissociation constants of ligand to the repressor with LBD in the active and inactive conformations, respectively, and c is ligand concentration. Partial binding of ligand is ignored in the symmetric model. All energy terms in the exponents are evaluated in the unit of $k_B T$.

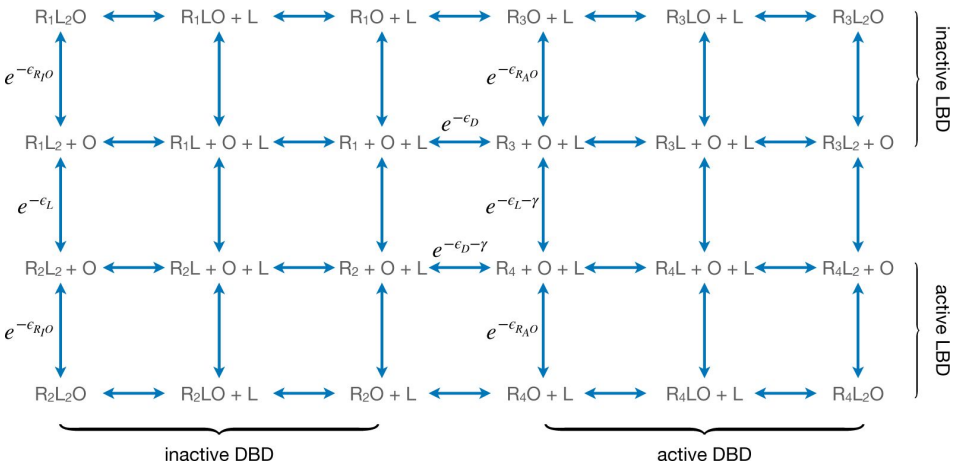

Figure 2—figure supplement 2.

Equilibria among different conformational and binding states of the repressor. Here, L and O represent ligand and operator respectively. ε_{R0} and ε_{R0} are the A I free energies of operator binding for repressor with DBD in the active and inactive conformation, respectively. R_1, R_2, R_3 and R_4 denote the L_I D_I, L_A D_I, L_I D_A and L_A D_A state of the repressor, respectively. All energy terms in the exponents are evaluated in the unit of $k_B T$.

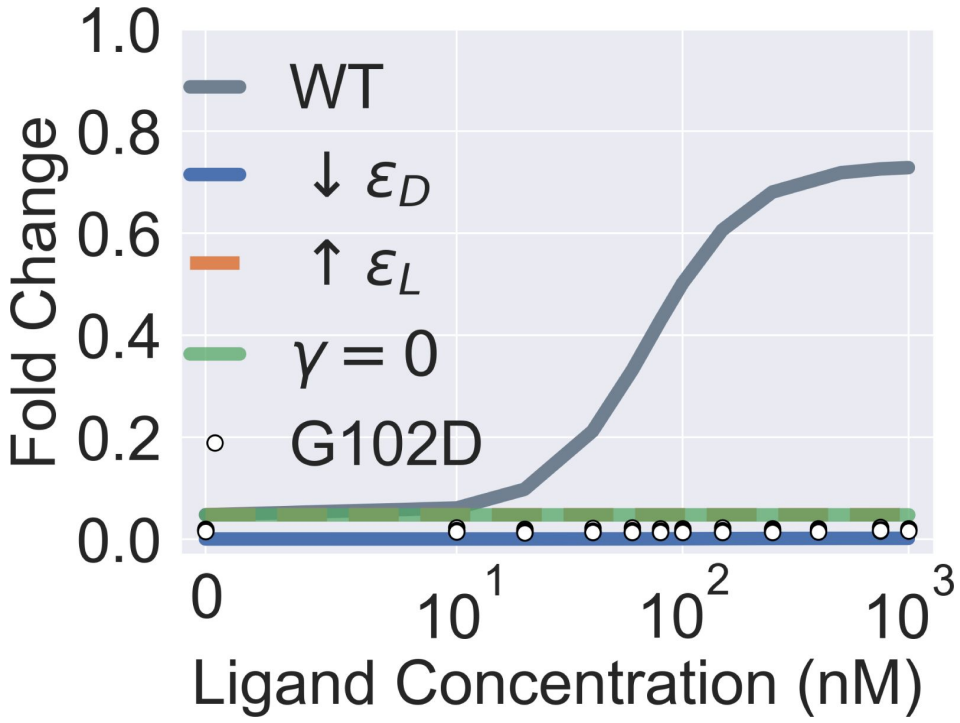

Figure 2—figure supplement 3.

Extended parametric study of main text ***Equation 1***. The four colored curves show that a flat induction curve can result from tuning each one of the three main biophysical parameters of the two-domain model alone (by decreasing ε_D or increasing ε_L from the WT value, or by setting γ to 0). The white points show the experimental induction data for the mutant G102D (measurements of 4 biological replicates at each ligand concentration). Note that the colored curves in the figure are generated for better visualization of the model parameters' effect on the induction curve and not to be compared with the experimental data of G102D. The leakiness of G102D (0.0173) is higher than that of the WT (0.0086) determined in experiments.

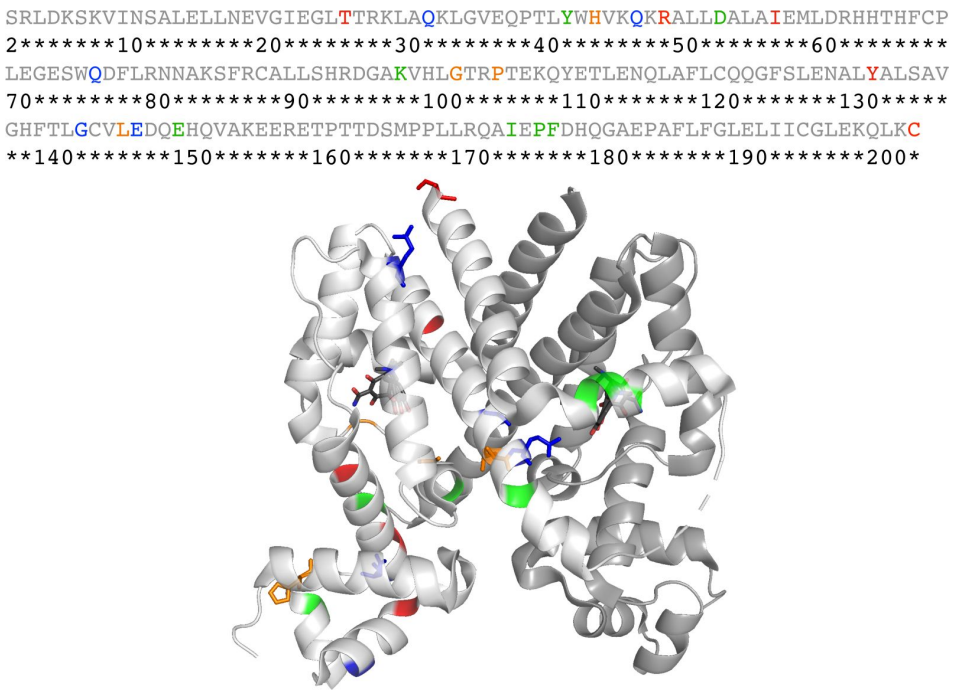

Figure 3—figure supplement 1.

Sequence and structural distributions of the 21 residues chosen for the mutation analyses in this work. The upper panel shows the sequence of TetR (residue 2-203), where the 21 residues chosen for mutation analyses in this work are colored red, orange, green or blue (while the other residues are colored grey). The lower panel shows the crystal structure of TetR(B) in complex with minocycline and magnesium (PDB code: 4AC0). Here, the two identical monomers of TetR are colored white and grey respectively, while the residues chosen for mutation analyses are colored in the same way as in the sequence above in the white monomer. Specifically, the 5 red residues from top to bottom are C203, Y132, I57, R49 and T26. The 4 orange residues from left to right are H44, P105, G102 and L146. The 5 blue residues from top to bottom are Q76, G143, E147, Q47 and Q32. The 7 green residues from left to right are Y42, D53, K98, E150, F177, P176 and I174. Some of the 21 residues are presented in the stick format to aid visualization while all other residues are presented in the cartoon format.

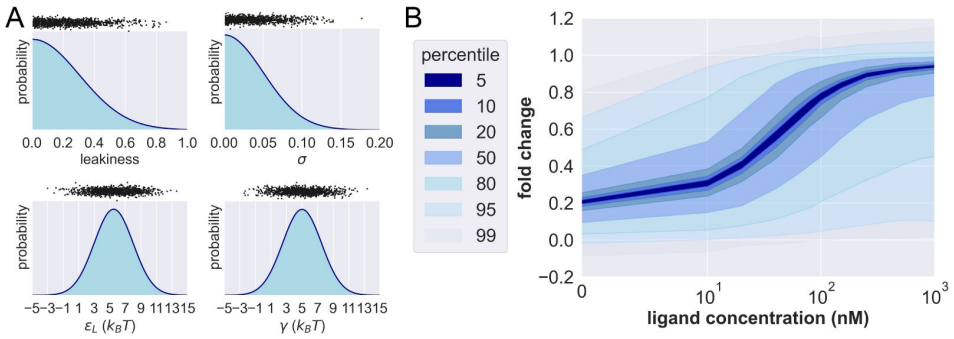

Figure 3—figure supplement 2.

Prior probability distributions and prior predictive check. (A) Density functions of the prior distributions of leakiness, σ, ε_L and γ. The black dots above the prior distributions show the 1000 prior predictive draws of the corresponding parameter. (B) Percentiles of the simulated fold changes using the 1000 sets of parameters shown in (A).

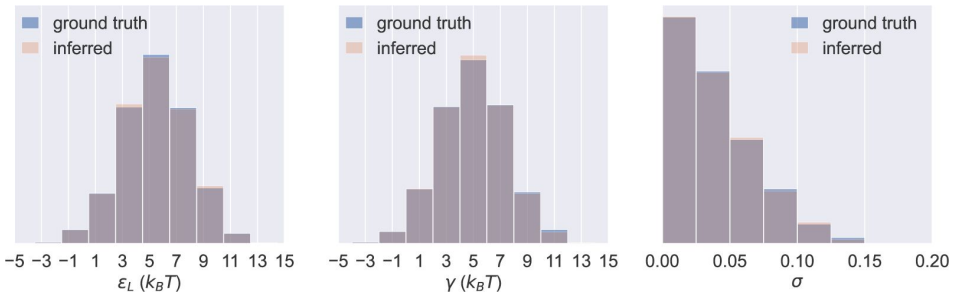

Figure 3—figure supplement 3.

Probability distributions of ε_L, γ and σ values in the 1000 sets of prior predictive draws (ground truth) and the average of the corresponding 1000 sets of inferred posterior distributions of the parameters (inferred).

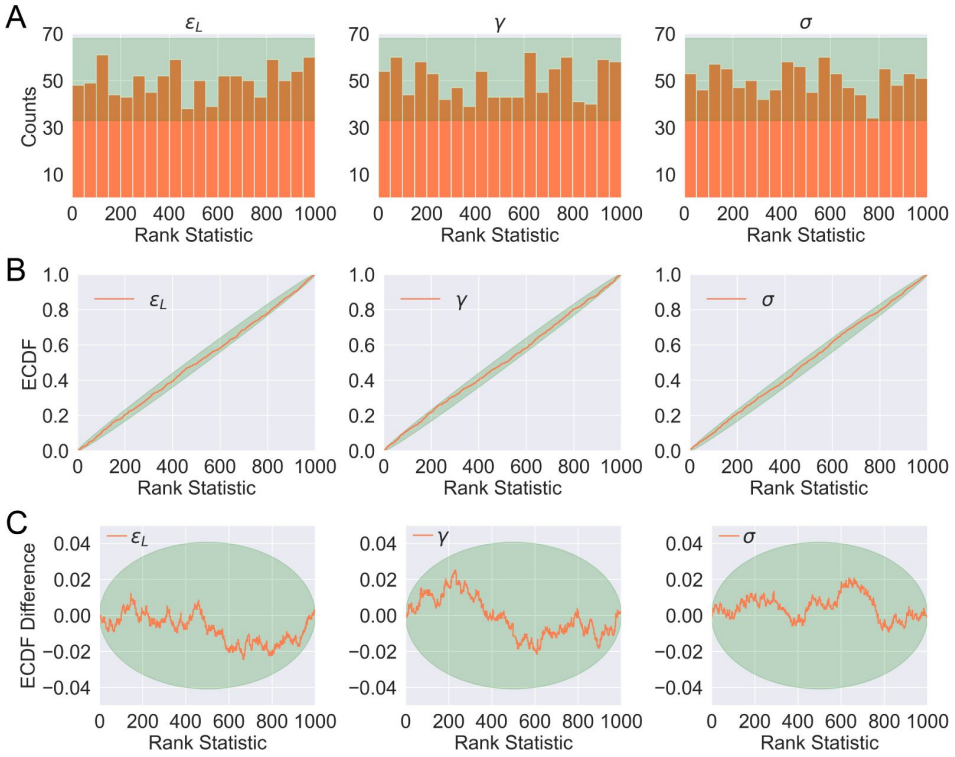

Figure 3—figure supplement 4.

Distributions of rank statistics of the prior predictive draws relative to the corresponding posterior samples. (A) Histograms (20 bins); (B) ECDF plots; (C) ECDF difference plots of rank statistics of ε_L, γ and σ. The green bands in (A)-(C) show the 99^{th}percentile expected from a true uniform distribution.

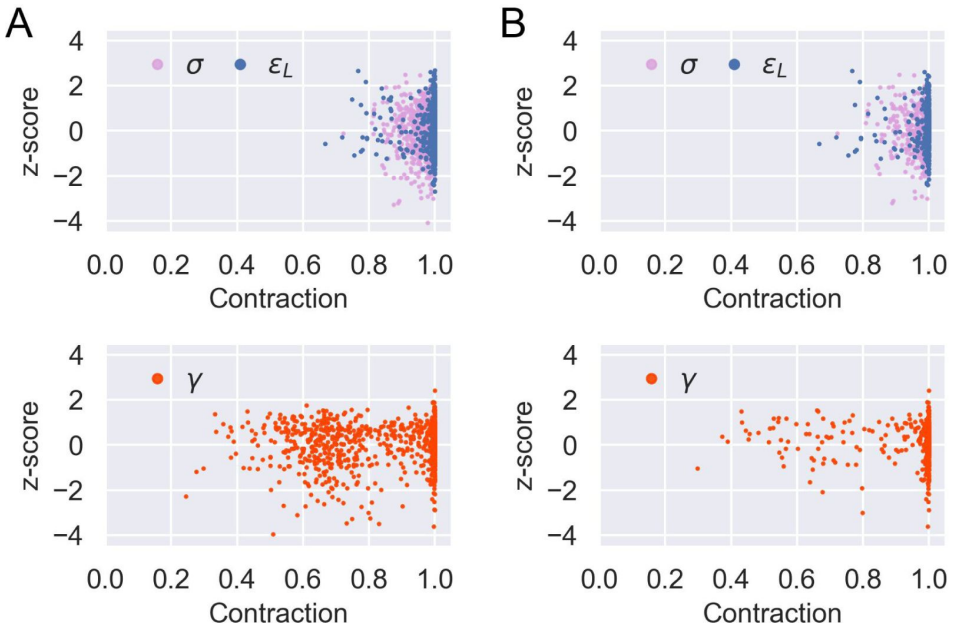

Figure 3—figure supplement 5.

Sensitivity analysis for model parameter inference. Posterior z-score and posterior contraction of the inferred posterior distribution for each of the 1000 prior predictive draws of parameters and the corresponding simulated data except: (A) parameters of flat induction curves (see Supplementary file section 3 and Eq. (32)); (B) parameters of flat induction curves or μ(c=1000 nM)>0.97 (see Supplementary file section 3 and Eq. (34)). Accordingly, there are 970 and 523 data points for each parameter in (A) and (B), respectively.

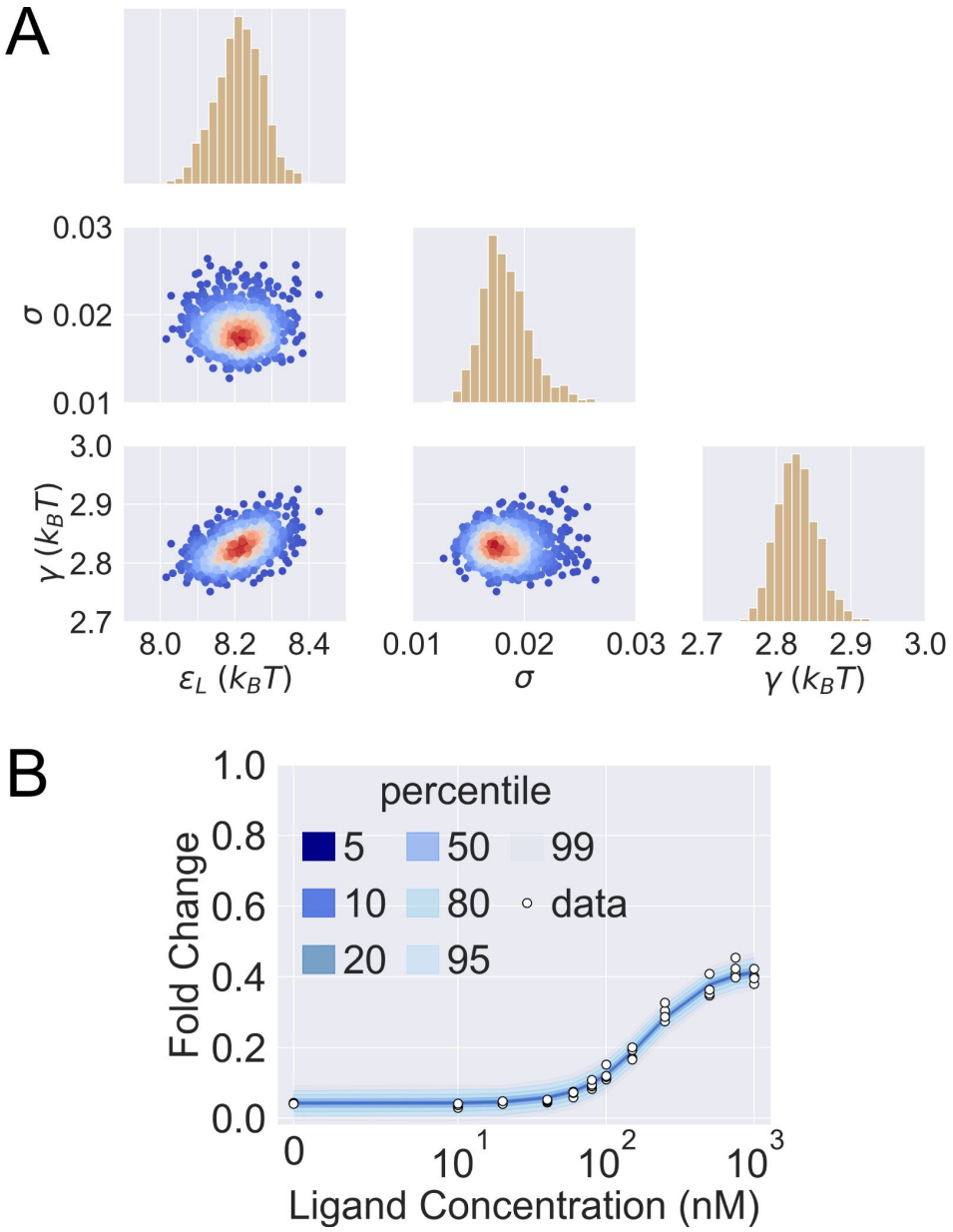

Figure 3—figure supplement 6.

Posterior predictive check of mutant G102D-Y42M-I57N. (A) 1000 sets of posterior samples of $\{\varepsilon, \gamma, \sigma\}$. The scattered plots show the joint distributions of the parameters, colored by the log probability of the parameter combinations. Blue/red corresponds to low/high probability. The histograms show the marginal distributions of the corresponding individual parameters. (B) Percentiles of the simulated fold change measurements using the 1000 sets of posterior samples based on Supplementary file Eq. (24). The white data points show the experimental induction data of four biological replicates.

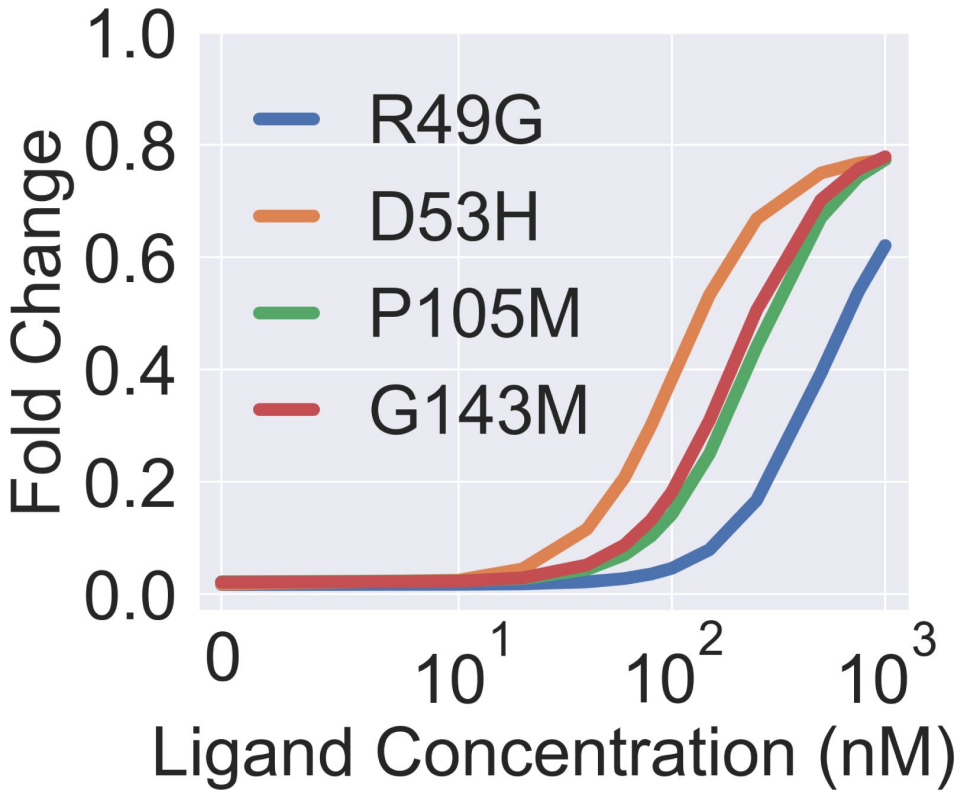

Figure 3—figure supplement 7.

Theoretical induction curves of the four dead mutants when their γ values are set to the WT value while using their respective ε_D and ε_L values (taken from **Figure 3B** in the main text). The theoretical induction curve is calculated with main text ***Equation 1***

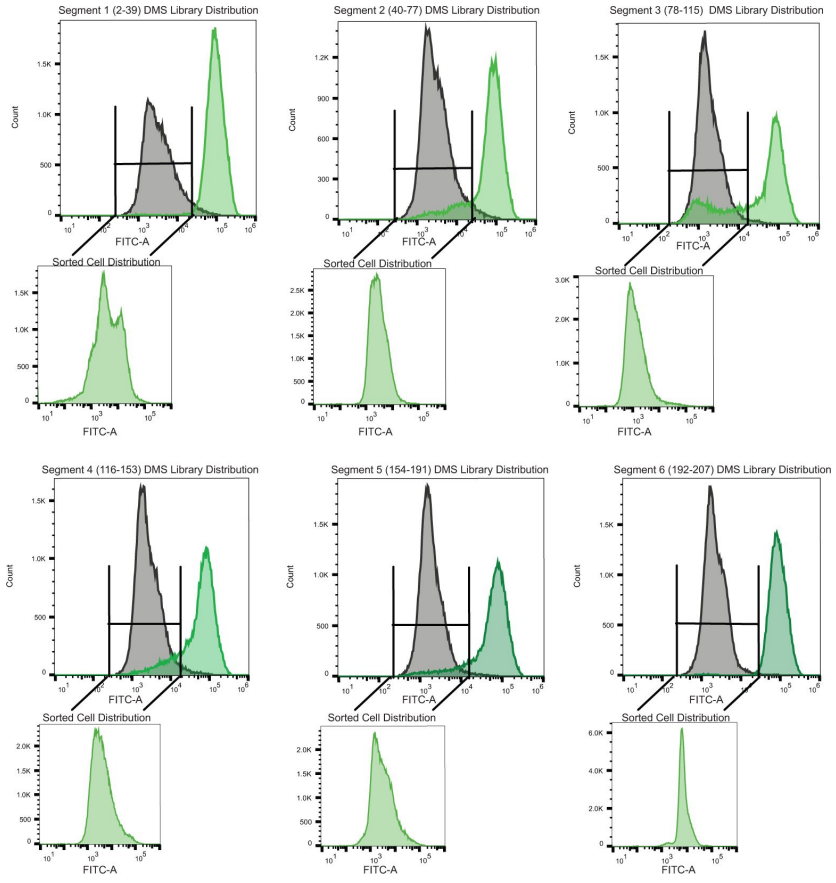

Figure 3—figure supplement 8.

Sorting scheme to identify dead variants. Each panel is a tiled segment of single site saturation mutants of defined length along the TetR gene. The residue number spanning each segment is shown above the panel. The gray distribution denotes the uninduced population of cells containing mutants. The dark green distribution on the same panel denotes the population of cells responding to the anhydrotetracycline. The uninduced population of cells containing mutants when was added was sorted and reflowed which is shown outside the main panel as the light green distribution.

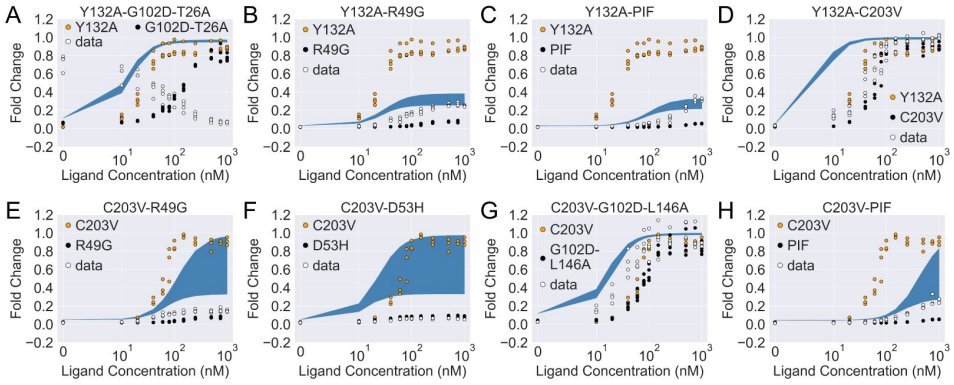

Figure 4—figure supplement 1.

The induction curves of the eight combined mutants calculated using the basic additive model (i.e., with $\alpha_{1,p} = \alpha_{2,p} = 1$ in main text ***Equation 4***). In each plot, the white data points show the experimental induction data of the combined mutants, while the black and orange ones show data of the individual mutants. The blue band show the 95^{th}percentile of the induction curve prediction from the additive model.

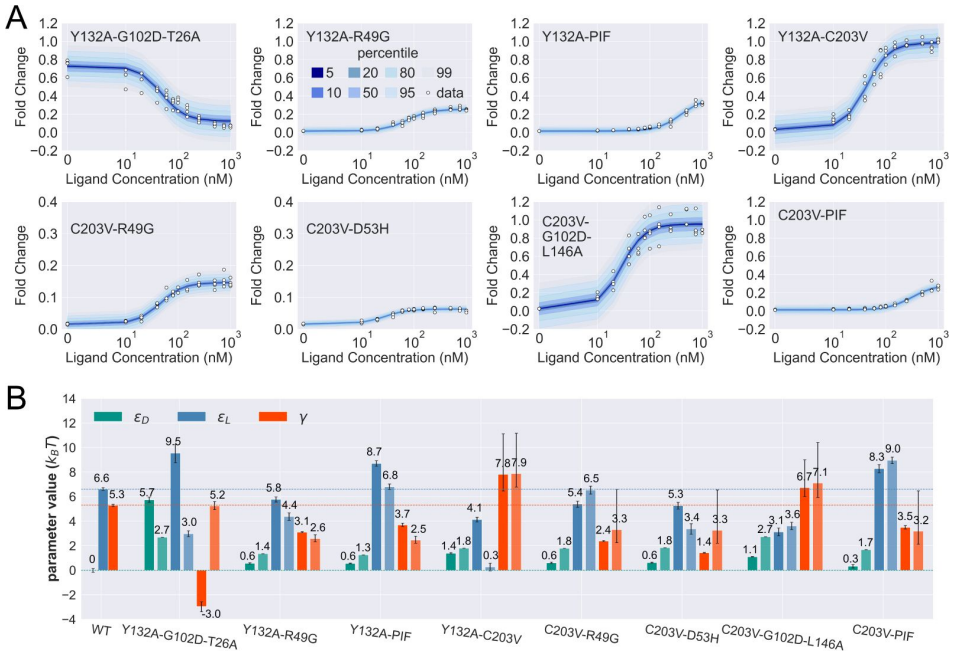

Figure 4—figure supplement 2.

Induction curves of the eight combined mutants and the corresponding parameter estimation results as well as the basic additive model predictions. (A) Percentiles of the simulated fold change measurements using the inferred posterior parameters of each mutant based on Supplementary file Eq. (24). The white data points show the experimental induction data of four biological replicates (three replicates for C203V-PIF). (B) The inferred parameter values of WT and the 8 combined mutants. Error bars of ε_L and γ represent the upper and lower bounds of the 95 percent credible region. For each combined mutant, the parameters shown by the lighter and darker bar plots are the results from the basic additive model and direct fitting, respectively. The horizontal lines show the WT parameter values for reference.

References

Amor BRC, Schaub MT, Yaliraki SN, Barahona M (2016) **Prediction of allosteric sites and mediating interactions through bond-to-bond propensities** *Nature Communications* **7**

Bacon F (1965) **On the nature of allosteric transitions: a plausible model** *J Mol Biol* **12**:88–118

Bolintineanu DS, Volzing K, Vivcharuk V, Sayyed-Ahmad A, Srivastava P, Kaznessis YN (2014) **Investigation of Changes in Tetracycline Repressor Binding upon Mutations in the Tetracycline Operator** *Journal of Chemical and Engineering Data* **59**:3167–3176

Brewster RC, Weinert FM, Garcia HG, Song D, Rydenfelt M, Phillips R (2014) **The Transcription Factor Titration Effect Dictates Level of Gene Expression** *Cell* **156**:1312–1323

Changeux JP (2012) **Allostery and the Monod-Wyman-Changeux model after 50 years** *Annual review of biophysics* **41**:103–133

Changeux JP, Edelstein SJ (2005) **Allosteric mechanisms of signal transduction** *Science* **308**:1424–1428

Chure G, Razo-Mejia M, Belliveau NM, Einav T, Kaczmarek ZA, Barnes SL, Lewis M, Phillips R (2019) **Predictive shifts in free energy couple mutations to their phenotypic consequences** *Proceedings of the National Academy of Sciences of the United States of America* **116**:18275–18284

Cui Q, Karplus M (2008) **Allostery and cooperativity revisited** *Protein science* **17**:1295–1307

Cuthbertson L, Nodwell JR (2013) **The TetR Family of Regulators** *Microbiology and Molecular Biology Reviews* **77**:440–475

Daber RD, Sochor M, Lewis M (2011) **Thermodynamic analysis of mutant lac repressors** *Journal of molecular biology* **409**:76–87

Daily MD, Gray JJ (2009) **Allosteric communication occurs via networks of tertiary and quaternary motions in proteins** *PLoS computational biology* **5**

Dokholyan NV (2016) **Controlling allosteric networks in proteins** *Chemical reviews* **116**:6463–6487

East KW, Newton JC, Morzan UN, Narkhede YB, Acharya A, Skeens E, Jogl G, Batista VS, Palermo G, Lisi GP (2019) **Allosteric motions of the CRISPR–Cas9 HNH nuclease probed by NMR and molecular dynamics** *Journal of the American Chemical Society* **142**:1348–1358

Eaton WA (2022) **A retrospective on statistical mechanical models for hemoglobin allostery** *The Journal of Chemical Physics* **157**

Faure AJ, Domingo J, Schmiedel JM, Hidalgo-Carcedo C, Diss G, Lehner B (2022) **Mapping the energetic and allosteric landscapes of protein binding domains** *Nature* **604**:175–183

Flynn JM, Rossouw A, Cote-Hammarlof PA, Fragata I, Mavor D, Hollins C, Bank C, Bolon DNA (2019) **Comprehensive fitness maps of Hsp90 show widespread environmental dependence** *eLife* **9**

Fowler DM, Araya CL, Fleishman SJ, Kellogg EH, Stephany JJ, Baker D, Fields S (2010) **High-resolution mapping of protein sequence-function relationships** *Nature Methods* **7**:741–746

Fowler DM, Fields S (2014) **Deep mutational scanning: a new style of protein science** *Nature Methods* **11**:801–807

Fukami-Kobayashi K, Tateno Y, Nishikawa K (2003) **Parallel evolution of ligand specificity between LacI/GalR family repressors and periplasmic sugar-binding proteins** *Molecular biology and evolution* **20**:267–77

Garcia HG, Phillips R (2011) **Quantitative dissection of the simple repression input–output function** *Proceedings of the National Academy of Sciences* **108**:12173–12178

Gunasekaran K, Ma B, Nussinov R (2004) **Is allostery an intrinsic property of all dynamic proteins?** *Proteins: Structure, Function, and Bioinformatics* **57**:433–443

Guo J, Zhou HX (2016) **Protein allostery and conformational dynamics** *Chemical reviews* **116**:6503–6515

Hecht B, Müller G, Hillen WPD (1993) **Noninducible Tet repressor mutations map from the operator binding motif to the C terminus** *Journal of Bacteriology* **175**:1206–1210

Henry ER *et al.* (2020) **Allosteric control of hemoglobin S fiber formation by oxygen and its relation to the patho-physiology of sickle cell disease** *Proceedings of the National Academy of Sciences* **117**:15018–15027

Hilser VJ, Wrabl JO, Motlagh HN (2012) **Structural and energetic basis of allostery** *Annual review of biophysics* **41**:585–609

Hu H, Howard RJ, Bastolla U, Lindahl E, Delarue M (2020) **Structural basis for allosteric transitions of a multidomain pentameric ligand-gated ion channel** *Proceedings of the National Academy of Sciences* **117**:13437–13446

Huss P, Meger A, Leander M, Nishikawa K, Raman S (2021) **Mapping the functional landscape of the receptor binding domain of T7 bacteriophage by deep mutational scanning** *eLife* **10**

Jones EM *et al.* (2020) **Structural and functional characterization of G protein–coupled receptors with deep mutational scanning** *eLife* **9**

Kamionka A, Bogdanska-Urbaniak J, Scholz O, Hillen WPD (2004) **Two mutations in the tetracycline repressor change the inducer anhydrotetracycline to a corepressor** *Nucleic acids research* **32**:842–847

Jr DE Koshland, Némethy G, Filmer D (1966) **Comparison of experimental binding data and theoretical models in proteins containing subunits** *Biochemistry* **5**:365–385

Kosuri S, Goodman DB, Cambray G, Mutalik VK, Gao Y, Arkin AP, Endy D, Church GM (2013) **Composability of regulatory sequences controlling transcription and translation in Escherichia coli** *Proceedings of the National Academy of Sciences* **110**:14024–14029

Kędracka-Krok S, Wasylewski Z (1999) **Kinetics and Equilibrium Studies of Tet Repressor–Operator Interaction** *Journal of Protein Chemistry* **18**:117–125

Leander M, Liu Z, Cui Q, Raman S (2022) **Deep mutational scanning and machine learning reveal structural and molecular rules governing allosteric hotspots in homologous proteins** *eLife* **11**

Leander M, Yuan Y, Meger A, Cui Q, Raman S (2020) **Functional plasticity and evolutionary adaptation of allosteric regulation** *Proceedings of the National Academy of Sciences* **117**:25445–25454

Lee J, Natarajan M, Nashine VC, Socolich M, Vo T, Russ WP, Benkovic SJ, Ranganathan R (2008) **Surface sites for engineering allosteric control in proteins** *Science*

Li X, Lehner B (2020) **Biophysical ambiguities prevent accurate genetic prediction** *Nature Communications* **11**

Lipscomb WN, Kantrowitz ER (2012) **Structure and mechanisms of Escherichia coli aspartate transcarbamoylase** *Accounts of chemical research* **45**:444–453

Liu J, Nussinov R (2008) **Allosteric effects in the marginally stable von Hippel–Lindau tumor suppressor protein and allostery-based rescue mutant design** *Proceedings of the National Academy of Sciences* **105**:901–906

Liu J, Nussinov R (2016) **Allostery: an overview of its history, concepts, methods, and applications** *PLoS computational biology* **12**

Lockless SW, Ranganathan R (1999) **Evolutionarily conserved pathways of energetic connectivity in protein families** *Science* **286**:295–299

Marzen S, Garcia HG, Phillips R (2013) **Statistical mechanics of monod–wyman–changeux (mwc) models** *Journal of molecular biology* **425**:1433–1460

McCormick JW, Russo MA, Thompson S, Blevins A, Reynolds KA (2021) **Structurally distributed surface sites tune allosteric regulation** *eLife* **10**

Motlagh HN, Wrabl JO, Li J, Hilser VJ (2014) **The ensemble nature of allostery** *Nature* **508**:331–339

Müller G, Hecht B, Helbl V, Hinrichs W, Saenger W, Hillen WPD (1995) **Characterization of non-inducible Tet repressor mutants suggests conformational changes necessary for induction** *Nature Structural Biology* **2**:693–703

Nierzwicki L, East KW, Morzan UN, Arantes PR, Batista VS, Lisi GP, Palermo G (2021) **Enhanced specificity mutations perturb allosteric signaling in CRISPR-Cas9** *Elife* **10**

Normanno D, Boudarène L, Dugast-Darzacq C, Chen J, Richter C, Proux F, Bénichou O, Voituriez R, Darzacq X, Dahan M (2015) **Probing the target search of DNA-binding proteins in mammalian cells using TetR as model searcher** *Nature Communications* **6**

Ota N, Agard DA (2005) **Intramolecular signaling pathways revealed by modeling anisotropic thermal diffusion** *Journal of molecular biology* **351**:345–54

Pan Y, Ma B, Venkataraghavan RB, Levine AJ, Nussinov R (2005) **In the quest for stable rescuing mutants of p53: computational mutagenesis of flexible loop L1** *Biochemistry* **44**:1423–1432

Pedelacq J, Cabantous S, Tran TH, Terwilliger TC, Waldo GS (2006) **Engineering and characterization of a superfolder green fluorescent protein** *Nature Biotechnology* **24**:79–88

Peracchi A, Mozzarelli A, 1814 (2011) **Exploring and exploiting allostery: Models, evolution, and drug targeting** *Biochimica et Biophysica Acta (BBA)-Proteins and Proteomics* **8**:922–933

Ramos JL, Martínez-Bueno M, Molina-Henares AJ, Terán W, Watanabe K, Zhang X, Gallegos MT, Brennan R, Tobes R (2005) **The TetR family of transcriptional repressors** *Microbiology and molecular biology reviews* **69**:326–356

Razo-Mejia M, Barnes SL, Belliveau NM, Chure G, Einav T, Lewis M, Phillips R (2017) **Tuning Transcriptional Regulation through Signaling: A Predictive Theory of Allosteric Induction** *Cell systems* **6**:456–469

Reichheld SE, Yu Z, Davidson AR (2009) **The induction of folding cooperativity by ligand binding drives the allosteric response of tetracycline repressor** *Proceedings of the National Academy of Sciences* **106**:22263–22268

Reynolds KA, McLaughlin RN, Ranganathan R (2011) **Hot Spots for Allosteric Regulation on Protein Surfaces** *Cell* **147**:1564–1575

Rodriguez GJ, Yao R, Lichtarge O, Wensel TG (2010) **Evolution-guided discovery and recoding of allosteric pathway specificity determinants in psychoactive bioamine receptors** *Proceedings of the National Academy of Sciences* **107**:7787–7792

Rydenfelt M, Cox RS, Garcia HG, Phillips R (2014) **Statistical mechanical model of coupled transcription from multiple promoters due to transcription factor titration. Physical review E** *Statistical, nonlinear, and soft matter physics* **89**

Sarkisyan KS *et al.* (2016) **Local fitness landscape of the green fluorescent protein** *Nature* **533**:397–401

Sauguet L, Shahsavar A, Delarue M, 1850 (2015) **Crystallographic studies of pharmacological sites in pentameric ligandgated ion channels** *Biochimica et biophysica acta* **3**:511–523

Scholz O *et al.* (2004) **Activity reversal of Tet repressor caused by single amino acid exchanges** *Molecular Microbiology* **53**

Scholz O, Schubert P, Kintrup M, Hillen WPD (2000) **Tet repressor induction without Mg2+** *Biochemistry* **39**:10914–10920

Schubert P, Pfleiderer K, Hillen WPD. (2004) **Tet repressor residues indirectly recognizing anhydrotetracycline** *European journal of biochemistry* **271**:2144–2152

Schueler-Furman O, Wodak SJ (2016) **Computational approaches to investigating allostery** *Current Opinion in Structural Biology* **41**:159–171

Sevvana M, Goetz C, Goeke D, Wimmer C, Berens C, Hillen W, Muller YA (2012) **An exclusive α/β code directs allostery in TetR–peptide complexes** *Journal of molecular biology* **416**:46–56

Starr TN *et al.* (2020) **Deep Mutational Scanning of SARS-CoV-2 Receptor Binding Domain Reveals Constraints on Folding and ACE2 Binding** *Cell* **182**:1295–1310

Strickland D, Moffat K, Sosnick TR (2008) **Light-activated DNA binding in a designed allosteric protein** *Proceedings of the National Academy of Sciences* **105**:10709–10714

Süel GM, Lockless SW, Wall MA, Ranganathan R (2003) **Evolutionarily conserved networks of residues mediate allosteric communication in proteins** *Nature structural biology* **10**:59–69

Szabo A, Karplus M (1972) **A mathematical model for structure-function relations in hemoglobin** *Journal of molecular biology* **72**:163–197

Tack DS, Tonner PD, Pressman A, Olson ND, Levy SF, Romantseva EF, Alperovich N, Vasilyeva O, Ross D (2021) **The genotype-phenotype landscape of an allosteric protein** *Molecular Systems Biology* **17**

Takeuchi K, Imai M, Shimada I (2019) **Conformational equilibrium defines the variable induction of the multidrug-binding transcriptional repressor QacR** *Proceedings of the National Academy of Sciences* **116**:19963–19972

Tonner PD, Pressman AD, Ross D (2021) **Interpretable modeling of genotype–phenotype landscapes with state-of-the-art predictive power** *Proceedings of the National Academy of Sciences of the United States of America* **119**

Tzeng SR, Kalodimos CG (2012) **Protein activity regulation by conformational entropy** *Nature* **488**:236–240

Velyvis A, Yang YR, Schachman HK, Kay LE (2007) **A solution NMR study showing that active site ligands and nucleotides directly perturb the allosteric equilibrium in aspartate transcarbamoylase** *Proceedings of the National Academy of Sciences* **104**:8815–8820

Viappiani C, Abbruzzetti S, Ronda L, Bettati S, Henry ER, Mozzarelli A, Eaton WA (2014) **Experimental basis for a new allosteric model for multisubunit proteins** *Proceedings of the National Academy of Sciences* **111**:12758–12763

Walker AS, Russ WP, Ranganathan R, Schepartz A (2020) **RNA sectors and allosteric function within the ribosome** *Proceedings of the National Academy of Sciences* **117**:19879–19887

Wang J, Jain A, McDonald LR, Gambogi C, Lee AL, Dokholyan NV (2020) **Mapping allosteric communications within individual proteins** *Nature communications* **11**

Weinert FM, Brewster RC, Rydenfelt M, Phillips R, Kegel WK (2014) **Scaling of gene expression with transcription-factor fugacity** *Physical review letters* **113**

Wodak SJ *et al.* (2019) **Allostery in its many disguises: from theory to applications** *Structure* **27**:566–578

Xie J, Zhang W, Zhu X, Deng M, Lai L (2022) **Coevolution-based prediction of key allosteric residues for protein function regulation** *eLife* **12**

Xu C, Tobi D, Bahar I (2003) **Allosteric changes in protein structure computed by a simple mechanical model: hemoglobin T R2 transition** *Journal of molecular biology* **333**:153–168

Yu EW, Koshland Jr DE (2001) **Propagating conformational changes over long (and short) distances in proteins** *Proceedings of the National Academy of Sciences* **98**:9517–9520

Yuan Y, Deng J, Cui Q (2022) **Molecular Dynamics Simulations Establish the Molecular Basis for the Broad Allostery Hotspot Distributions in the Tetracycline Repressor** *Journal of the American Chemical Society*

Article and author information

Zhuang Liu
Department of Physics, Boston University, Boston, United States
ORCID iD: 0000-0003-4695-7142

Thomas Gillis
Department of Biochemistry, University of Wisconsin, Madison, United States

Srivatsan Raman
Department of Biochemistry, University of Wisconsin, Madison, United States, Department of Chemistry, University of Wisconsin, Madison, United States, Department of Bacteriology, University of Wisconsin, Madison, United States
ORCID iD: 0000-0003-2461-1589

Qiang Cui
Department of Physics, Boston University, Boston, United States, Department of Chemistry, Boston University, Boston, United States
For correspondence: qiangcui@bu.edu
ORCID iD: 0000-0001-6214-5211

Copyright

Editors

Reviewing Editor
Shozeb Haider
University College London, London, United Kingdom

Senior Editor
Amy Andreotti
Iowa State University, Ames, United States of America

Reviewer #1 (Public Review):

Summary:

The authors' earlier deep mutational scanning work observed that allosteric mutations in TetR (the tetracycline repressor) and its homologous transcriptional factors are distributed across the structure instead of along the presumed allosteric pathways as commonly expected. Especially, in addition, the loss of the allosteric communications promoted by those mutations, was rescued by additional distributed mutations. Now the authors develop a two-domain thermodynamic model for TetR that explains these compelling data. The model is consistent with the in vivo phenotypes of the mutants with changes in parameters, which permits quantification. Taken together their work connects intra- and inter-domain allosteric regulation that correlate with structural features. This leads the authors to suggest broader applicability to other multidomain allosteric proteins.

Here the authors follow their first innovative observations with a computational model that captures the structural behavior, aiming to make it broadly applicable to multidomain proteins. Altogether, an innovative and potentially useful contribution.

Weaknesses:

None that I see, except that I hope that in the future, if possible, the authors would follow with additional proteins to further substantiate the model and show its broad applicability. I realize however the extensive work that this would entail.

https://doi.org/10.7554/eLife.92262.2.sa1

Reviewer #2 (Public Review):

Summary:

This combined experimental-theoretical paper introduces a novel two-domain statistical thermodynamic model (primarily Equation 1) to study allostery in generic systems but focusing here on the tetracycline repressor (TetR) family of transcription factors. This model, building on a function-centric approach, accurately captures induction data, maps mutants with precision, and reveals insights into epistasis between mutations.

Strengths:

The study contributes innovative modeling, successful data fitting, and valuable insights into the interconnectivity of allosteric networks, establishing a flexible and detailed framework for investigating TetR allostery. The manuscript is generally well-structured and communicates key findings effectively.

Comments on revised version:

I am happy with the changes made by the authors

https://doi.org/10.7554/eLife.92262.2.sa0

Author response:

The following is the authors' response to the previous reviews.

We greatly appreciate the comments from the editor and the reviewers, based on which we have made the revisions. We have responded to all the questions and summarized the revisions below. The changes are also highlighted in the manuscript.

Additionally, we've noticed a few typos in the manuscript presented on the eLife website, which were not there in our originally submitted file.

> *(1) In both the "Full text" presented on the eLife website and the pdf file generated after clicking "Download": the last FC1000 in the second paragraph of the "Extensive induction curves fitting of TetR mutants" section should be FC1000WT .*
>
> *(2) In the pdf file generated after clicking "Download": the brackets are all incorrectly formatted in the captions of Figure 4 and Figure 3—figure supplement 6.*
>
> ***eLife assessment***
>
> *The fundamental study presents a two-domain thermodynamic model for TetR which accurately predicts in vivo phenotype changes brought about as a result of various mutations. The evidence provided is solid and features the first innovative observations with a computational model that captures the structural behavior, much more than the current single-domain models.*

We appreciate the supportive comments by the editor and reviewers.

> ***Public Reviews:***
>
> ***Reviewer #1 (Public Review):***
>
> *Summary:*
>
> *The authors' earlier deep mutational scanning work observed that allosteric mutations in TetR (the tetracycline repressor) and its homologous transcriptional factors are distributed across the structure instead of along the presumed allosteric pathways as commonly expected. Especially, in addition, the loss of the allosteric communications promoted by those mutations, was rescued by additional distributed mutations. Now the authors develop a two-domain thermodynamic model for TetR that explains these compelling data. The model is consistent with the in vivo phenotypes of the mutants with changes in parameters, which permits quantification. Taken together their work connects intra- and inter-domain allosteric regulation that correlate with structural features. This leads the authors to suggest broader applicability to other multidomain allosteric proteins. Here the authors follow their first innovative observations with a computational model that captures the structural behavior, aiming to make it broadly applicable to multidomain proteins. Altogether, an innovative and potentially useful contribution.*

We thank the reviewer for the supportive comments.

> *Weaknesses:*
>
> *None that I see, except that I hope that in the future, if possible, the authors would follow with additional proteins to further substantiate the model and show its broad applicability. I realize however the extensive work that this would entail.*

We thank the reviewer for the supportive comments and the suggestion to extend the model to other proteins, which we indeed plan to pursue in future studies.

> ***Reviewer #2 (Public Review):***
>
> *Summary:*

> *This combined experimental-theoretical paper introduces a novel two-domain statistical thermodynamic model (primarily Equation 1) to study allostery in generic systems but focusing here on the tetracycline repressor (TetR) family of transcription factors. This model, building on a function-centric approach, accurately captures induction data, maps mutants with precision, and reveals insights into epistasis between mutations.*
>
> *Strengths:*
>
> *The study contributes innovative modeling, successful data fitting, and valuable insights into the interconnectivity of allosteric networks, establishing a flexible and detailed framework for investigating TetR allostery. The manuscript is generally well-structured and communicates key findings effectively.*

We thank the reviewer for the supportive comments.

> *Weaknesses:*
>
> *The only minor weakness I found was that I still don't have a better sense into (a) intuition and (b) mathematical derivation of Equation 1, which is so central to the work. I would recommend that the authors provide this early on in the main text.*

We thank the reviewer for the suggestion. The full mathematical derivation of Equation 1 is given in the first section of the supplementary file. Given the length of the derivation, we think it's better to keep it in the supplementary file rather than the main text. In the main text, the first subsection (overview of the two-domain thermodynamic model of allostery) of the Results section and the paragraph right before Equation 1 are meant for providing intuitive understandings of the two-domain model and the derivation of Equation 1, respectively.

We would also like to point the reviewer to Figure 2-figure supplement 2 and Equations (12) to (18) in the supplementary file for an alternative derivation. They show that the equilibria among all molecular species containing the operator are dictated by the binding free energies, the ligand concentration, and the allosteric parameters. The probability of an unbound operator (proportional to the probability that the promoter is bound by a RNA polymerase, or the gene expression level) can thus be calculated using Equation (12), which then leads to main text Equation 1 following the derivation given there.

Additionally, we've added a paragraph to the main text (line 248-260) to aid an intuitive understanding of Equation 1.

"The distinctive roles of the three biophysical parameter on the induction curve as stipulated in Equation 1 could be understood in an intuitive manner as well. First, the value of ε_D controls the intrinsic strength of binding of TetR to the operator, or the intrinsic difficulty for ligand to induce their separation. Therefore, it controls how tightly the downstream gene is regulated by TetR without ligands (reflected in leakiness) and affects the performance limit of ligands (reflected in saturation). Second, the value of ε_L controls how favorable ligand binding is in free energy. When ε_L increases, the binding of ligand at low concentrations become unfavorable, where the ligands cannot effectively bind to TetR to induce its separation from the operator. Therefore, the fold-change as a function of ligand concentration only starts to noticeably increase at higher ligand concentrations, resulting in larger EC50. Third, as discussed above, γ controls the level of anti-cooperativity between the ligand and operator binding of TetR, which is the basis of its allosteric regulation. In other words, γ controls how strongly ligand binding is incompatible with operator binding for TetR, hence it controls the performance limit of ligand (reflected in saturation)."

We hope that the reviewer will find this explanation helpful.

> ***Reviewer #3 (Public Review):***
>
> *Summary:*
>
> *Allosteric regulations are complicated in multi-domain proteins and many large-scale mutational data cannot be explained by current theoretical models, especially for those that are neither in the functional/allosteric sites nor on the allosteric pathways. This work provides a statistical thermodynamic model for a two-domain protein, in which one domain contains an effector binding site and the other domain contains a functional site. The authors build the model to explain the mutational experimental data of TetR, a transcriptional repress protein that contains a ligand and a DNA-binding domain. They incorporate three basic parameters, the energy change of the ligand and DNA binding domains before and after binding, and the coupling between the two domains to explain the free energy landscape of TetR's conformational and binding states. They go further to quantitatively explain the in vivo expression level of the TetR-regulated gene by fitting into the induction curves of TetR mutants. The effects of most of the mutants studied could be well explained by the model. This approach can be extended to understand the allosteric regulation of other two-domain proteins, especially to explain the effects of widespread mutants not on the allosteric pathways. Strengths: The effects of mutations that are neither in the functional or allosteric sites nor in the allosteric pathways are difficult to explain and quantify. This work develops a statistical thermodynamic model to explain these complicated effects. For simple two-domain proteins, the model is quite clean and theoretically solid. For the real TetR protein that forms a dimeric structure containing two chains with each of them composed of two domains, the model can explain many of the experimental observations. The model separates intra and inter-domain influences that provide a novel angle to analyse allosteric effects in multi-domain proteins.*

We thank the reviewer for the supportive comments.

> *Weaknesses:*
>
> *As mentioned above, the TetR protein is not a simple two-main protein, but forms a dimeric structure in which the DNA binding domain in each chain forms contacts with the ligand-binding domain in the other chain. In addition, the two ligand-binding domains have strong interactions. Without considering these interactions, especially those mutants that are on these interfaces, the model may be oversimplified for TetR.*

We thank the reviewer for this valid concern and acknowledge that TetR is a homodimer. However, we've deliberately chosen to simplify this complexity in our model for the following reasons.

(1) In this work, we aim to build a minimalist model for two-domain allostery withonly the most essential parameters for capturing experimental data. The simplicity of the model helps promote its mechanistic clarity and potential transferability to other allosteric systems.

(2) Fewer parameters are needed in a simpler model. Our two-domain modelcurrently uses only three biophysical parameters, which are all demonstrated to have distinct influences on the induction curve (see the main text section "System-level ramifications of the two-domain model"). This enables the inference of parameters with high precision for the mutants, and the quantification of the most essential mechanistic effects of their mutations, provided that the model is shown to accurately recapitulate the comprehensive dataset. Thus, we found it was unnecessary to add another parameter for explicitly describing inter-chain coupling, which would likely incur uncertainty in the inference of parameters due to the redundancy of their effects on induction data, and prevent the model from making faithful predictions.

(3) From a more biological point of view, TetR is an obligate dimer, meaning thatthe two chains must synchronize for function, supporting the two-domain simplification of TetR for binding concerns.

Additionally, as shown in the subsection “Inclusion of single-ligand-bound state of repressor” of section 1 of the supplementary file, incorporating the dimeric nature of TetR in our model by allowing partial ligand binding does not change the functional form of main text equation 1 in any practical sense. Therefore, considering all the factors stated above, we think that increasing the complexity of the two-domain model will only be necessary if additional data emerge to suggest the limitation of our model.

> ***Recommendations for the authors:***
>
> ***Reviewer #1 (Recommendations For The Authors):***
>
> *This is an excellent work. I have only one suggestion for the authors. Interestingly, the authors also note that the epistatic interactions that they obtain are consistent with the structural features of the protein, which is not surprising. Within this framework, have the authors considered rescue mutations? Please see for example PMID: 18195360 and PMID: 15683227. If I understand right, this might further extend the applicability of their model. If so, the authors may want to add a comment to that effect.*

We thank the reviewer for the supportive comments and for pointing us to the useful references. We have added some comments to the main text regarding this point in line 332-336: “The diverse mechanistic origins of the rescuing mutations revealed here provide a rational basis for the broad distributions of such mutations. Integrating such thermodynamic analysis with structural and dynamic assessment of allosteric proteins for efficient and quantitative rescuing mutation design could present an interesting avenue for future research, particularly in the context of biomedical applications (PMID: 18195360, PMID: 15683227).”

> ***Reviewer #3 (Recommendations For The Authors):***
>
> *The authors should try to build a more realistic dimeric model for TetR to see if it could better explain experimental data. If it were too complicated for a revision, more discussions on the weakness of the current model should be given.*

We thank the reviewer for this valid concern and for the suggestion. The reasons for refraining from increasing the complexity of the model are fully discussed in our response to the reviewer’s public review given above. Primarily, we think that the value of a simple physical model is two-fold (e.g., the paradigm Ising model in statistical physics and the classic MWC model), first, its mechanistic clarity and potential transferability makes it a useful conceptual framework for understanding complex systems and establishing universal rules by comparing seemingly unrelated phenomena; second, it provides useful insights and design principles of specific systems if it can quantitatively capture the corresponding experimental data. Thus, given the current experimental data set, we believe it is justified to keep the two-domain model in its current form, while additional experimental data could necessitate a more complex model for TetR allostery in the future. Relevant discussions are added to the main text (line 443-446) and section 8 of the supplementary file.

“It’s noted that the homodimeric nature of TetR is ignored in the current two-domain model to minimize the number of parameters, and additional experimental data could necessitate a more complex model for TetR allostery in the future (see supplementary file section 8 for more discussions).”

> *Minor issues:*
>
> *(1) There is an error in Figure 3A, the 13th and 14th subgraphs are the same and should be corrected.*

We thank the reviewer for capturing this error, which has been corrected in the revised manuscript.

> *(2) The criteria for the selection of mutants for analysis should be clearly given. Apart from deleting mutants that are in direct contact with the ligand of DNA, how many mutants are left, and how far are they are from the two sites? In line 257, what are the criteria for selecting these 15 mutants? Similarly, in line 332, what are the criteria for selecting these 8 mutants?*

We thank the reviewer for this comment. The data selection criteria are now added in section 7 of the supplementary file. The distances to the DNA operator and ligand of the 21 residues under mutational study are now added in Table 1 (Figure 3-figure supplement 9). The added materials are referenced in the main text where relevant.

"7. Mutation selection for two-domain model analysis

In this work, there are 24 mutants studied in total including the WT, and they contain mutations at 21 WT residues. We did not perform model parameter inference for the mutant G102D because of its flat induction curve (see the second subsection of section 2 and main text Figure 2—figure Supplement 3). Therefore, there are 23 mutants analyzed in main text Figure 5.

Measuring the induction curve of a mutant involves a significant amount of experimental effort, which therefore is hard to be extended to a large number of mutants. Nonetheless, we aim to compose a set of comprehensive induction data here for validating our two-domain model for TetR allostery. To this end, we picked 15 individual mutants in the first round of induction curve measurements, which contains mutations spanning different regions in the sequence and structure of TetR (main text Figure 3—figure Supplement 1). Such broad distribution of mutations across LBD, DBD and the domain interface could potentially lead to diverse induction curve shapes and mutant phenotypes for validating the two-domain model. Indeed, as discussed in the main text section "Extensive induction curves fitting of TetR mutants", the diverse effects on induction curve from mutations perturbing different allosteric parameters predicted by the model, are successfully observed in these 15 experimental induction curves. Additionally, 5 of the 15 mutants contain a dead-rescue mutation pair, which helps us validate the model prediction that a dead mutation could be rescued by rescuing mutations that perturb the allosteric parameters in various ways.

Eight mutation combinations were chosen for the second round of induction curve measurement for studying epistasis, where we paired up C203V and Y132A with mutations from different regions of the TetR structure. Such choice is largely based on two considerations. 1. As both C203V and Y132A greatly enhance the allosteric response of TetR, we want to probe why they cannot rescue a range of dead mutations as observed previously (PMID: 32999067). 2. C203V and Y132A are the only two mutants that show enhanced allosteric response in the first round of analysis. Combining detrimental mutations of allostery in a combined mutant could potentially lead to near flat induction curve, which is less useful for inference (see the second subsection of section 2)."

> *Since the number of hotspots identified by DMS is not very large, why not analyze them all?*

We thank the reviewer for this comment. There are 41 hotspot residues in TetR (PMID: 36226916), which have 41*19=779 possible single mutations. It's unfeasible to perform induction curve measurements for all of these 779 mutants in our current experiment. However, we agree that it would be helpful if we can obtain such a dataset in an efficient way.

> *In line 257, there are 15 mutants mentioned, while in Figure 5, there are 23 mutants mentioned, in Figure 3-figure supplement 1, there are 21 mutants mentioned, and in line 226 of the supplementary file, there are 24 mutants mentioned, which is very confusing. Therefore, the data selection criteria used in this article should be given.*

We thank the reviewer for this comment. The data selection criteria are now given in section 7 of the supplementary file, which should clarify this confusion.

> *(3) In Figure 4 of the Exploring epistasis between mutations section, the 6 weights of the additive models corresponding to each mutation combination are different. On one hand, it seems that there are no universal laws in these experimental data. On the other hand, unique parameters of a single mutation combination were not validated in other mutation combinations, which somewhat weakened the conclusions about the potential physical significance of these additive weights.*

We thank the reviewer for this comment. We admit that a quantitative universal law for tuning the 6 weights of the additive model does not manifest in our data, which indicates the mutation-specific nature of epistatic interactions in TetR as hinted in the different rescuing mutation distributions of different dead mutations (PMCID: PMC7568325). However, clear common trends in the weight tuning of combined mutants that contain common mutations do emerge, which comply with the structural features of the protein and provide explanations as to why C203V and Y132A don't rescue a range of dead mutations (main text section "Exploring epistasis between mutations"). Additionally, the lack of a quantitative universal rule for tuning the 6 weights in our simple model doesn't exclude the possibility of the existence of universal law for epistasis in TetR in another functional form, a point that could be explored in the future with more extensive joint experimental and computational investigations.

> *In Eq. (27) of the supplementary file, the prior distribution of inter-domain coupling γ is given as a Gaussian distribution centered at 5 kBT. Since the absolute value of γ is important, can the authors explain why the prior distribution of γ is set to this value and what happens if other values are used?*

We thank the reviewer for the question. As explained in the corresponding discussions of Eq. (27) in the supplementary file, the prior of γ is chosen to serve as a soft constraint on its possible values based on the consideration that 1. inter-domain energetics for a TetR-like protein should be on the order of a few kBT; and 2. the prior distribution should reflect the experimental observation in the literature that γ has a small probability of adopting negative values upon mutations. Given our thorough validation of the statistical model and computational algorithm (see section 3 of the supplementary file), and the high precision in the parameter fitting results using experimental data (Figure 3 and Figure 4-figure supplement 2), we conclude that 1. the physical range of parameters encoded in their chosen prior distributions agrees well with the value reflected in the experimental data; 2. the inference results are predominantly informed by the data. Thus, changing the mean of the prior distribution of γ should not affect the inference results significantly given that it remains in the physical range.

This point is explicitly shown in the added Table 2 (Figure 3-figure supplement 10), where we compare the current Bayesian inference results with those obtained after increasing the standard deviation of the Gaussian prior of γ from 2.5 to 5 kBT. As shown in the table, most inference results stay virtually unchanged at the use of this less informative prior, which confirms that they are predominantly informed by the data. The only exceptions are the slight increase of the inferred γ values for C203V, C203V-Y132A and C203V-G102D-L146A, reflecting the intrinsic difficulty of precise inference of large γ values with our model, as is already discussed in the second subsection of section 3 of the supplementary file. However, such observations comply with the common trend of epistatic interactions involving C203V presented in the main text and don't compromise the ability of our model to accurately capture the induction curves of mutants. Relevant discussions are now added to the second subsection of section 3 of the supplementary file (line 368-385).

"In our experimental dataset, such inference difficulty is only observed in the case of C203V, Y132A-C203V and C203V-G102D-L146A due to their large γ and γ + εL values (see main text Figure 3, Figure 3—figure Supplement 10 and Figure 4). As shown in main text Figure 3—figure Supplement 10, the inference results for the other 20 mutants stay highly precise and virtually unchanged after increasing the standard deviation of the Gaussian prior of γ ($gstd\gamma$) from 2.5 to 5 kBT. This demonstrates that the inference results for these mutants are strongly informed by the induction data and there is no difficulty in the precise inference of the parameter values. On the other hand, the inferred γ values (especially the upper bound of the 95% credible region) for C203V, Y132A-C203V and C203V-G102D-L146A increased with $gstd\gamma$. This is because the induction curves in these cases are not sensitive to the value of γ given that it's large enough as discussed above. Hence, when unphysically large γ values are permitted by the prior distribution, they could enter the posterior distribution as well. Such difficulty in the precise inference of γ values for these three mutants however, doesn't compromise the ability of our model in accurately capturing the comprehensive set of induction data (see part iv below). Additionally, the increase of the inferred γ value of C203V at the use of larger $gstd\gamma$ complies with the results presented in main text Figure 4, which show that the effect of C203V on γ tends to be compromised when combined with mutations closer to the domain interface."